Projected Seasonal Changes in Large-Scale Global Precipitation and Temperature Extremes Based on the CMIP5 Ensemble

WANG ZHAN AND XIAOGANG HE

Department of Civil and Environmental Engineering, Princeton University, Princeton, New Jersey

JUSTIN SHEFFIELD

Geography and Environmental Sciences, University of Southampton, Southampton, United Kingdom

ERIC F. WOOD

Department of Civil and Environmental Engineering, Princeton University, Princeton, New Jersey

(Manuscript received 6 June 2019, in final form 6 December 2019)

ABSTRACT

Over the past decades, significant changes in temperature and precipitation have been observed, including changes in the mean and extremes. It is critical to understand the trends in hydroclimatic extremes and how they may change in the future as they pose substantial threats to society through impacts on agricultural production, economic losses, and human casualties. In this study, we analyzed projected changes in the characteristics, including frequency, seasonal timing, and maximum spatial and temporal extent, as well as severity, of extreme temperature and precipitation events, using the severity–area–duration (SAD) method and based on a suite of 37 climate models archived in phase 5 of the Coupled Model Intercomparison Project (CMIP5). Comparison between the CMIP5 model estimated extreme events and an observation-based dataset [Princeton Global Forcing (PGF)] indicates that climate models have moderate success in reproducing historical statistics of extreme events. Results from the twenty-first-century projections suggest that, on top of the rapid warming indicated by a significant increase in mean temperature, there is an overall wetting trend in the Northern Hemisphere with increasing wet extremes and decreasing dry extremes, whereas the Southern Hemisphere will have more intense wet extremes. The timing of extreme precipitation events will change at different spatial scales, with the largest change occurring in southern Asia. The probability of concurrent dry/hot and wet/hot extremes is projected to increase under both RCP4.5 and RCP8.5 scenarios, whereas little change is detected in the probability of concurrent dry/cold events and only a slight decrease of the joint probability of wet/cold extremes is expected in the future.

1. Introduction

Understanding the changing characteristics of climate extremes (e.g., droughts, floods, heat waves, and cold spells) is critical, as they pose substantial threats to water (Palmer 2013), food (Wheeler and Von Braun 2013; Lobell and Gourdji 2012; He et al. 2019), energy (Mideksa and Kallbekken 2010), and economic security (Mendelsohn et al. 2006; Stern 2013). Significant changes in the mean state of temperature T and precipitation P have been well documented (e.g., Easterling et al. 2000; Alexander 2016). There is also evidence that their extreme states are becoming more frequent and intense (e.g., Goswami et al. 2006; Barriopedro et al. 2011; Seneviratne et al. 2012). For instance, there is medium confidence that the frequency and duration of heat waves/warm spells have increased over most land areas (IPCC 2013). Compared to temperature, historical changes in mean and extreme precipitation have been more uncertain and generally are not significant relative to natural variability (Alexander 2016). Nevertheless, significant increases in

Denotes content that is immediately available upon publication as open access.

Supplemental information related to this paper is available at the Journals Online website: https://doi.org/10.1175/JCLI-D-19-0311.s1.

Corresponding author: Wang Zhan, joyce.zhanwang@gmail.com

DOI: 10.1175/JCLI-D-19-0311.1

the magnitude of observed daily extreme precipitation have been reported in North America and high latitudes of the Northern Hemisphere (NH) (Trenberth 2011) as well as many other regions (see IPCC 2013; Alexander 2016). Looking into the future, a growing body of research indicates that the characteristics of temperature and precipitation extremes will continue to change under anthropogenic climate change (Sillmann et al. 2013b; Toreti et al. 2013; Trenberth et al. 2015). Furthermore, regional studies (e.g., Westra et al. 2013) have identified an increase in frequency and intensity of daily precipitation amounts based on climate extremes indices recommended by the World Meteorological Organization's (WMO's) Expert Team on Climate Change Detection and Indices (ETCCDI; Zhang et al. 2011).

Global climate models, also referred to as general circulation models (GCMs), are frequently used in climate studies. In general, GCMs have moderate success in reproducing historical climate statistics, with room for substantial improvement (Sillman et al. 2013a; Sheffield et al. 2013a,b; C. Wang et al. 2014). Errors in simulated temperature and precipitation remain large, especially in the tropics (Kharin et al. 2013; Aloysius et al. 2016). With the release of the most recent climate simulations from the state-of-the-art coupled GCMs involved in phase 5 of the Coupled Model Intercomparison Project (CMIP5; Taylor et al. 2012) and updated prescribed emission scenarios known as representative concentration pathways (RCPs; van Vuuren et al. 2011), further studies to advance our knowledge on projected climate extremes have been possible. Many studies have compared and evaluated the capability of the CMIP5 GCMs in simulating global (e.g., Sillmann et al. 2013a) and regional (e.g., Sheffield et al. 2013a,b) climate against gauge and satellite-based observations as well as reanalysis. Improved skill in CMIP5 compared to its predecessor CMIP3 (Meehl et al. 2007) confirms that updates to climate models do improve performance (Sillmann et al. 2013a). However, due to the inherent uncertainties of each single GCM, the multimodel, multiensemble average generally provides more reliable and robust estimates than each individual model (Tebaldi and Knutti 2007). Further efforts have also been made to select a subset of models to represent the mean and variability of climate change due to computational constraints or the need to exclude poorly performing models (e.g., Evans et al. 2013, 2014; Cannon 2015).

To date, a number of studies have investigated the changing behavior of climate extremes (see above). A few studies have investigated in depth the range of characteristics of extremes, such as changes in the total occurrence, highest severity, longest duration, and maximum spatial extent. These are important because, for example, the maximum extent of an extreme is of great relevance to regional impact assessment as well as mitigation and adaptation strategies for decision makers. Among the few relevant studies, Vidal et al. (2012) found that the frequency, total magnitude, mean duration, and area of meteorological drought events in France will increase in the twenty-first century based on the downscaled climate projections from the ARPEGE GCM under three emission scenarios taken from the Special Report on Emissions Scenarios (SRES; Nakicenovic and Swart 2000). Through a regional case study, Barriopedro et al. (2011) found that summer mega-heatwaves in Europe with similar magnitude and spatial extent as the 2003 and 2010 events will be 5–10 times more likely in the coming 40 years. Besides droughts and heatwaves, there are many other studies examining the changing characteristics (e.g., frequency and long-term trend) of the flip side of these extremes, including floods (or wet extremes; Milly et al. 2002; Hirabayashi et al. 2013; Arnell and Gosling 2016; He et al. 2020) and cold spells (e.g., Kodra et al. 2011; de Vries et al. 2012). More recently, there is a growing interest in compound events (e.g., joint occurrence of precipitation and temperature extremes), whose societal and environmental impacts can be exacerbated and exceed the sum of each individual type's impact (e.g., Leonard et al. 2014; Sarhadi et al. 2018), due to the nonlinear dependence structure (Zscheischler and Seneviratne 2017; Moftakhari et al. 2017; Hao et al. 2018). However, analysis in these studies is generally performed at the pixel level and ignores the dynamic nature of hydrological extremes, whose duration, severity, and spatial extent both evolve through space and time. Ignoring the spatial–temporal relationships in the interlinked characteristics of extremes may lead to an underestimation of the compounding impacts, especially under climate change, which influences not only the trend and variability of individual extremes, but also the joint dependence structure between different extremes. Our study aims to address this issue leveraging on recent advances in extreme event identification (e.g., see details below on the severity–area–duration analysis), which can identify spatially and temporally contiguous wet/dry and hot/cold extremes and how they merge or break up through space and time.

In this study, we investigate how univariate and bivariate climate extremes are expected to change in the future by analyzing the characteristics of extreme temperature and precipitation events over global land regions based on 37 climate model simulations carried out under the CMIP5 experiment. An extreme event is defined here as a multimonth and spatially extensive anomaly in precipitation and temperature, rather than a

daily or subdaily extreme value at the gridpoint scale, which is typically used in climate change studies. These large-scale events often have the largest impacts in human and economic terms and are thus worthy of studying. We compare the regional occurrence and characteristics of wet/dry and hot/cold extremes in the period 1961–2003, as represented by climate model historical simulations, to an observation-based dataset, Princeton Global Forcings (PGF; Sheffield et al. 2006). The near-term (2009–51) and long-term (2057–99) projections in the twenty-first century are evaluated relative to the historical period (1961–2003). Simulated changes in precipitation and temperature extremes, as well as concurrent dry/wet and hot/cold events from the 37 climate models under two future climate scenarios, RCP4.5 and RCP8.5, are analyzed to represent plausible emissions pathways.

2. Datasets

a. CMIP5 models

We use monthly precipitation and temperature data from the first ensemble member (r1i1p1) of 37 GCMs in the CMIP5 archive (Taylor et al. 2012). A list of the climate models used in this study is provided in Table S1 in the online supplemental material. We divide the twenty-first century into two 43-yr periods (January 2009–December 2051 and January 2057–December 2099) and compare each projection period relative to the historical period (January 1961–December 2003) of the same length for the two emission scenarios (van Vuuren et al. 2011), RCP4.5 (moderate emission) and RCP8.5 (high emission). RCP4.5 assumes stabilized radiative forcing at 4.5 $W m^{-2}$, equivalent to approximately 650 ppm CO_2, in the year 2100 without ever exceeding that value (Thomson et al. 2011), while RCP8.5 assumes the highest rate of increased greenhouse gas concentrations within this set of RCPs. All temperature and precipitation data are preprocessed to have the same 0.5° × 0.5° spatial resolution using bilinear interpolation to match the PGF data.

b. Observation-based dataset

The observational reference precipitation and temperature are obtained from the surface meteorological data from the V2 version of the PGF dataset (Sheffield et al. 2006), which consists of 3-hourly, 0.25° resolution fields of near-surface meteorology for global land areas from 1948 to 2010. PGF merges the NCEP–NCAR reanalysis with satellite–gauge precipitation from the Global Precipitation Climatology Project (GPCP; Adler et al. 2003), satellite-based precipitation from the Tropical Rainfall Measuring Mission (TRMM) Multisatellite Precipitation Analysis (TMPA; Huffman et al. 2007), the Climatic Research Unit (CRU) monthly precipitation and temperature gauge analyses (New et al. 2000; Harris et al. 2014), and the Surface Radiation Budget (SRB) radiation dataset (Stackhouse et al. 2004). PGF offers multiple variables that can be used to drive land surface models including precipitation, temperature, pressure, downward surface shortwave and longwave radiation, specific humidity, and wind speed. The dataset has been extensively used in regional and global studies of climate and hydrology applications (e.g., Sheffield and Wood 2008; Wang et al. 2011; He et al. 2020). PGF provides reliable, multidecadal information about the global climatology and variability of precipitation and temperature under current climate conditions. We aggregate this dataset to 0.5° and monthly resolution to match the climate model data.

3. Methods

a. Standardized indexes

We calculate standardized indices for both temperature and precipitation as indicators of dry/wet and cold/hot conditions for the observed and simulated historic periods, as well as the simulated future periods. Results are presented for 19 subcontinental land regions with different climatic regimes, covering the global land surface excluding Greenland (GRL), southeastern Asia (SEA), and extremely dry regions with annual rainfall amount less than 50 mm; that is, desert regions, including the Sahara, Arabian, Atacama, Iranian, and Taklamakan Deserts (Fig. 1). We do not consider the SEA region because our approach relies on analyzing spatially connected regions experiencing extremes, and this region is too disconnected to allow this. We adopt the subcontinental regions defined by Giorgi and Francisco (2000). Sheffield (2008) modified their GRL region to exclude the interior of Greenland and renamed GRL as northeastern Canada (NEC).

We calculate the standardized temperature index (STI) and standardized precipitation index (SPI) respectively for the historical period. The projections of STI and SPI for the twenty-first century are calculated based on the assumption that they have the same empirical cumulative probability distribution as the historical period. Procedures to calculate the SPI and STI are briefly described below.

1) STANDARDIZED PRECIPITATION INDEX

The SPI is a standardized measure of precipitation departure based on the empirical probability distribution

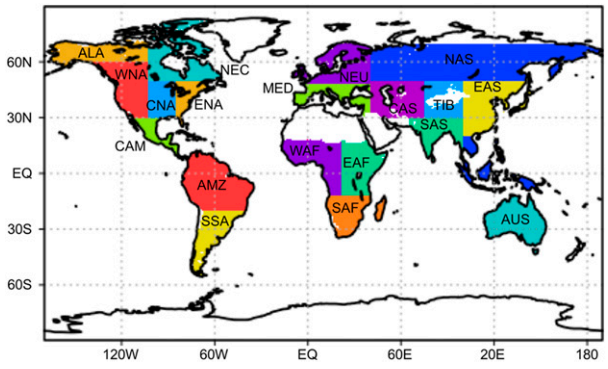

FIG. 1. Map showing the 19 subcontinental climate regions used in the analysis. ALA: Alaska; WNA: western North America; CNA: central North America; ENA: eastern North America; NEC: northeastern Canada; CAM: central America; AMZ: Amazon; SSA: southern South America; MED: Mediterranean; NEU: northern Europe; WAF: western Africa; EAF: eastern Africa; SAF: southern Africa; NAS: northern Asia; CAS: central Asia; TIB: Tibet; SAS: southern Asia; EAS: eastern Asia; AUS: Australia.

function and can be calculated at various time scales allowing for aggregation of precipitation extremes at monthly to multiyear scales. It has been recommended by the World Meteorological Organization (WMO 2012) as the preferred drought indicator, but can equally represent extreme wet conditions. Mathematically, the precipitation time series of a given grid cell is modeled with a gamma distribution:

$$f(\alpha,\beta)=\frac{\beta^{\alpha}}{\Gamma(\alpha)}x^{\alpha-1}e^{-\beta x},$$

where $\Gamma(\cdot)$ is the gamma function, x is the precipitation amount at certain time scales (e.g., monthly), α is the shape parameter, and β is the scale parameter; α and β are estimated through maximum likelihood estimation. The cumulative probability of the gamma distribution is then transformed to the equivalent number of standard deviations assuming a standard normal distribution. Following the commonly used classification based on the SPI (McKee et al. 1993), we adopted a threshold value of −1.0 for drought and a value of 1.0 for floods, below (above) which a region is considered as dry (wet) conditions (He et al. 2020).

2) STANDARDIZED TEMPERATURE INDEX

The standardized temperature index (STI) is defined in a similar manner to the SPI by Hansen et al. (2012). It measures the deviation of temperature from the mean in units of standard deviation. Instead of a gamma distribution in the calculation of SPI, STI assumes a normal distribution for the anomaly of the temperature time series after removing the seasonal cycle (Hansen et al. 2012). It has been used previously as a temperature indicator in climate variability studies to understand the role of climate extremes (Zscheischler et al. 2014). We use the same SPI thresholds as defined for dry/wet conditions. That is, if a grid cell has a STI value smaller (larger) than −1 (1) in a specific month, it is recognized as experiencing a cold/hot wave.

b. Severity–area–duration analysis

The severity–area–duration (SAD) analysis (Andreadis et al. 2005) is used to define spatial–temporal drought risk (severity) but can equally be used to define flood risk. The analysis begins with the identification of spatial clusters of the extreme at each time step based on severity and spatial coherency. A grid cell is defined as experiencing an extreme event if it has a standardized index (SPI or STI) larger than 1 for wet/hot extremes (smaller than −1 for dry or cold extremes). Following the threshold value for a minimum cluster extent adopted in previous studies (Zhan et al. 2016; He et al. 2020), the algorithm identifies spatial clusters consisting of at least 150 spatially contiguous grid cells (equivalent to approximately 3.75×10^5 km^2) experiencing extreme conditions. The analysis is carried out for each of 19 subcontinental climate regions shown in Fig. 1. The identified clusters are then linked in time based on the extent of overlapping area between time steps. Following this step of temporal tracking, a number of extreme events are identified allowing for merging and splitting between clusters. The dry/wet and hot/cold clusters identified in the SAD analysis are also used to identify concurrent precipitation and temperature extreme events. After the extreme events are identified based on 3-month SPI (SPI3) or 3-month STI (STI3), we analyze the identified events with respect to frequency of occurrence, duration, and maximum area. It should be noted that our estimates are focused on seasonal extreme events using a 3-month window, as these events have larger impacts on long-term agricultural activities (e.g., irrigation, planting practices) and water management, although we acknowledge that week-scale heat waves and day-to-week-scale floods also have large societal impacts. Moreover, selection of a common temporal scale (i.e., 3 months) enables us to quantify and compare different types of extremes in a consistent way.

In the SAD analysis, severity S at time step t is defined as

$$S_t=1-\frac{\sum_{t}^{t-T+1}F(|\mathrm{SI}|)}{T},\quad \mathrm{SI}\in\{\mathrm{STI},\mathrm{SPI}\},$$

where $F(\cdot)$ denotes the cumulative probability density (assuming a standard normal distribution), T is predefined at a 3-month time scale, and SI denotes either SPI or STI depending on the variable in question. Prior to the SAD analysis, a median filter is applied to the severity maps for spatial smoothing, as done in the original SAD algorithm (Andreadis et al. 2005). The SAD analysis is conducted for each extreme event using the following steps:

(i) Locate the maximum severity grid cell, hereby referred to as the ''center''.
(ii) Identify the grid cell with the next highest severity that is contiguous to the center with severity that exceeds the threshold.
(iii) Search for the grid cell with the next highest severity that is contiguous to the grid cells currently identified, and calculate the average severity of the grid cells.
(iv) Continue adding the next most severe grid cells until all contiguous grids exceeding the threshold are included.

For a specified extreme event duration, the SAD curve is defined as the envelope of the most severe events as a function of the event extent (i.e., area), as shown in Fig. S1. The regional SAD envelope curve represents the most extreme spatiotemporal evolution of all extreme events for that particular region. It is usually composed of portions of different events that have the most severity over an area given the specified duration. Here we focus on the 3-month time scale ($t = 3$) only. Each point in the SAD envelope curve represents the maximum severity of its corresponding spatial extent and temporal duration. Further information on SAD analysis can be found in Andreadis et al. (2005).

4. Results

a. Simulated historical climate extremes

Comparing the cumulative distribution function (CDF) of monthly spatial extent of temperature and precipitation extremes in the twenty-first century in Fig. S2, the CDF curve based on PGF matches well with the CMIP5 multimodel ensemble mean for both temperature and precipitation extremes. Detailed time series showing future projected areas under temperature and precipitation extremes are shown in Figs. S3 and S4, respectively.

1) NUMBER OF DRY AND WET EVENTS

Table 1 summarizes the statistics of dry and wet events in terms of the 95% confidence interval of the multimodel ensemble. The frequency of regional short-term dry and wet extreme events is underestimated by the CMIP5 models except for a few regions that include AMZ, WNA, and ALA (see Fig. 1 for regions and abbreviations). NAS and NEC had the most occurrence of dry and wet events in the historical period. The occurrence of short-term (1–6-month duration) and midterm (7–11-month duration) events in NAS is underestimated while they are overestimated in NEC by the CMIP5 models. For long-term (12+-month duration) events, the frequency of regional precipitation extreme events is better reproduced by the CMIP5 models in extratropics in the Northern Hemisphere. Fewer dry and wet events are reproduced by the CMIP5 models in AUS due to more frequent occurrence of short to midterm events.

2) MAXIMUM SPATIAL EXTENT AND DURATION OF EXTREME EVENTS

Figure 2 shows the maximum duration and spatial extent of dry and wet extremes estimated by CMIP5 models. In general, the maximum spatial extent and temporal duration of the precipitation extreme events from the CMIP5 models are fairly consistent with results from the PGF derived SPI maps. The maximum duration of dry and wet extremes is relatively better estimated compared to the maximum spatial extent. The maximum duration of dry and wet extremes from the reference PGF dataset falls within 25th and 75th quantiles of the CMIP5 model estimates in 8 and 9 regions out of 19, respectively. Only 3 and 6 regions, respectively for dry and wet extremes, have an estimated interquartile range covering the observed maximum spatial extent for dry and wet extremes. The duration of the longest dry and wet extreme events is slightly overestimated by the CMIP5 models with larger differences in the high-latitude regions [e.g., underestimated maximum duration of wet extreme events in NEC]. On the other hand, the area of the most spatially extensive event is more accurately estimated, partly because this is bounded above at 1.0 (extreme events cover the entire region). Nevertheless, the maximum duration and spatial extent of individual events in the PGF generally lie within the range of the CMIP5 multimodel ensembles. Out of the 19 regions evaluated, the observed maximum duration (area) of wet extremes falls within one standard deviation of the climate model ensembles in 12 (11) regions. For dry extremes, the observed maximum duration (area) falls within 1 standard deviation of the climate model ensembles in 7 (5) regions. Larger discrepancies are found for wet extremes than dry extremes with overestimated maximum spatial and/or temporal extent in most regions except for ALA, AMZ, CNA, WNA and

TABLE 1. Number of short-term (1–6 month), midterm (7–11 month), and long-term (12+ month) dry and wet extreme events in PGF and CMIP5 models in the historical period (1961–2003). The 95% confidence interval of the estimated frequency by CMIP5 models is provided in parentheses.

	Dry			Wet		
	Short-term	Midterm	Long-term	Short-term	Midterm	Long-term
CAS	25 (33–37)	6 (8–9)	0 (1–2)	36 (38–43)	7 (8–9)	1 (1–1)
WAF	20 (37–41)	3 (7–9)	0 (0–1)	32 (39–43)	15 (7–9)	2 (0–1)
NEU	31 (40–44)	7 (7–9)	0 (1–1)	43 (42–46)	5 (8–9)	0 (1–1)
NAS	85 (72–79)	17 (22–25)	8 (7–8)	87 (77–83)	29 (23–25)	4 (8–9)
CNA	23 (26–29)	1 (5–6)	0 (0–1)	31 (30–33)	2 (4–6)	0 (0–1)
TIB	29 (30–34)	2 (2–3)	0 (0–0)	35 (32–35)	0 (3–4)	0 (0–0)
AUS	23 (26–30)	8 (8–10)	0 (2–3)	34 (35–39)	7 (8–10)	1 (2–3)
NEC	49 (64–68)	8 (7–8)	1 (0–1)	69 (74–78)	5 (6–8)	1 (0–1)
SAS	22 (28–31)	1 (4–6)	0 (0–1)	24 (35–38)	2 (4–5)	0 (0–0)
EAF	23 (33–37)	7 (7–9)	0 (1–2)	19 (36–40)	5 (7–9)	1 (1–2)
CAM	7 (16–18)	0 (1–2)	0 (0–0)	15 (19–21)	0 (1–2)	0 (0–0)
MED	24 (25–27)	2 (3–4)	0 (0–0)	25 (29–32)	1 (2–3)	0 (0–0)
EAS	38 (46–50)	8 (10–12)	0 (1–2)	42 (51–56)	7 (10–12)	0 (1–2)
SSA	29 (36–40)	4 (7–8)	1 (1–1)	42 (39–43)	2 (6–8)	0 (1–1)
ALA	39 (37–41)	7 (7–8)	1 (1–2)	48 (41–45)	9 (7–9)	1 (1–2)
ENA	25 (23–26)	0 (2–3)	0 (0–0)	20 (24–27)	2 (2–3)	0 (0–0)
SAF	17 (29–32)	2 (6–7)	0 (0–1)	30 (33–36)	5 (5–7)	0 (0–1)
AMZ	45 (35–40)	15 (11–13)	1 (3–4)	54 (40–46)	14 (12–14)	4 (3–4)
WNA	45 (42–46)	3 (11–12)	1 (1–2)	51 (44–48)	6 (10–12)	0 (1–2)

NAS. Regions with the largest uncertainty range of the maximum duration from CMIP5 models are NAS and AMZ. This is most likely because the two regions are relatively larger than the other regions (14.7×10^{12} and 12.9×10^{12} km^2, respectively), which allows for more diverse depiction of precipitation extremes.

3) SAD CURVES FOR DRY AND WET EXTREMES

Figures 3 and 4 show 3-month SAD envelope curves that represent the maximum severity across different spatial extents for dry and wet extremes, respectively. In general, the multimodel ensemble can well replicate the maximum severity of observed precipitation extremes. Exceptions include the overestimated severity of dry and wet extremes in SAS. The severity of wet extreme events is better estimated by the CMIP5 models than the dry extremes. The slight overestimation in the severity of dry extreme events is found in TIB, EAF, ALA, and CAM.

Overall, the CMIP5 multimodel ensemble has moderate success in estimating the trend and spatiotemporal characteristics of temperature and precipitation extreme events in the historical period (1961–2003). This provides us with moderate confidence in the reliability of the CMIP5 models in simulating extremes.

b. Projected future changes in temperature extremes

Figure S3 shows the projected time series of land area under hot and cold extremes in the near-term (2009–51) and long-term (2057–99) twenty-first century. It is clear that the spatial and temporal extent of hot events are projected to increase significantly in the next decades under the RCP4.5 emission scenario, which is consistent with many previous studies (e.g., Cheng et al. 2015). By the end of the twenty-first century, ~83.4% of the global land area is projected to experience high temperature above one standard deviation of the temperature climatology in the historical period, under the RCP4.5 emission scenario, while 86.7% is projected under the RCP8.5 emission scenario (see Fig. S3). On average, global air temperature is expected to increase by 1.43° and 4.79°C, from 10.75° to 12.18° and 15.54°C, respectively (shown in Fig. 5).

It is worth noting that there are seasonal variations of the fractional area experiencing hot and cold events (Fig. S3). This suggests that on top of the increasing trend in annual mean temperature, there is more rapid warming during June–August (JJA) than December–February (DJF) in the extratropics. Despite the fact that a warming trend tends to produce more statistical anomalies in summer than winter, differences in variability are more pronounced in winter seasons, producing a seasonal cycle in 1-sigma anomalies. In addition, the large difference in land area in the northern and southern hemispheres could also create a seasonal cycle at the global scale. Furthermore, the fractional area of hot extremes has stronger seasonal fluctuations compared to that for cold extremes in the Northern Hemisphere, which suggests asymmetry in projected increases in extreme temperature distributions in the Northern Hemisphere.

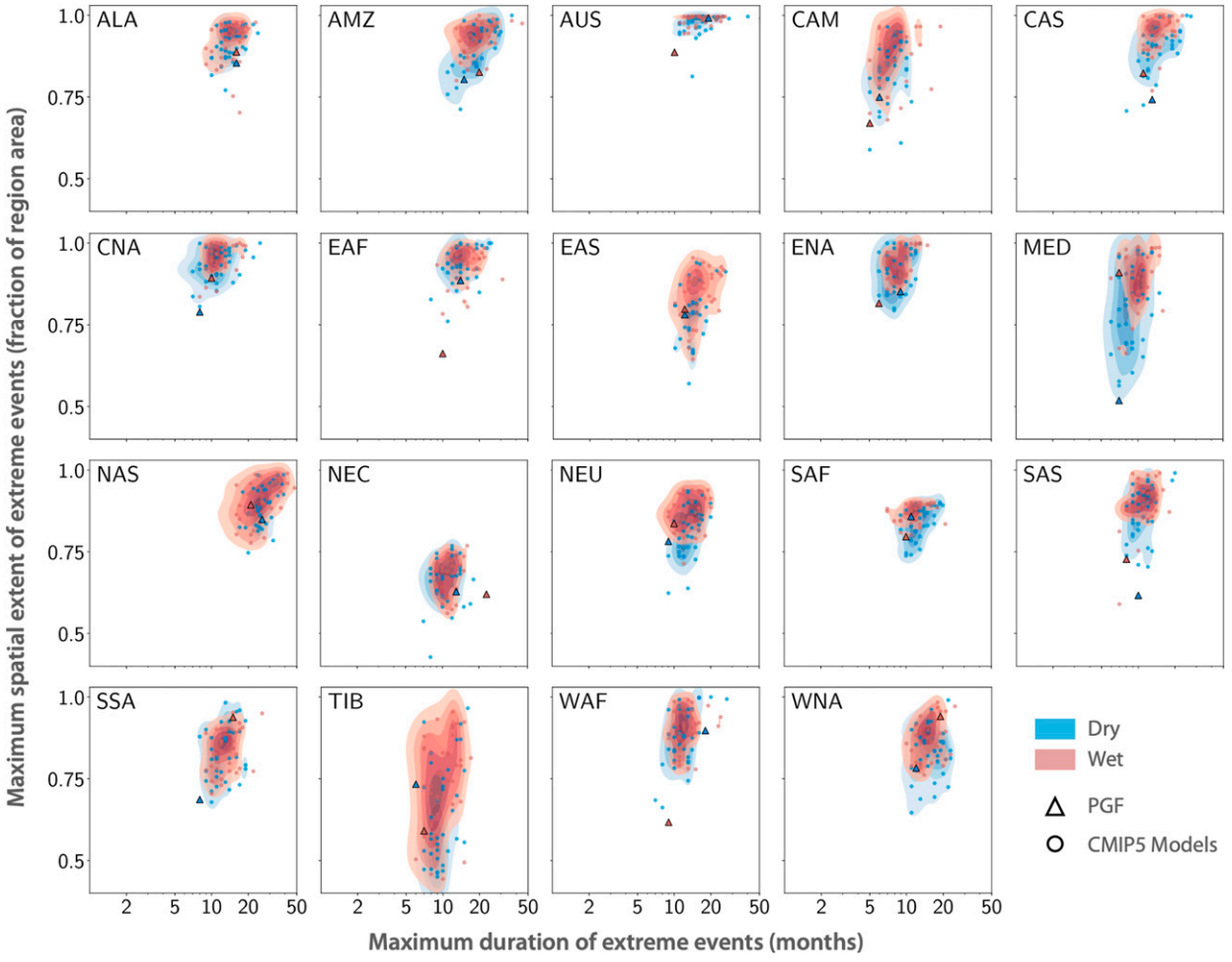

FIG. 2. Maximum temporal duration and maximum spatial extent for dry and wet extreme events in PGF and CMIP5 models during the historical period (1961–2003).

Stronger asymmetry is found in projections under the RCP8.5 scenario than RCP4.5 that has been noted previously (Kodra and Ganguly 2014). There is a longer upper tail found in the projected temperature distribution in JJA than in DJF (as illustrated in Fig. 13), indicating a larger increase in JJA temperature variability than DJF temperature as compared to the historical period.

c. *Projected future changes in precipitation extremes*

Figure S4 shows the time series of projected spatial extent for dry and wet extremes in the twenty-first century. Globally, by 2099, the spatiotemporal extent of dry events will slightly decrease, while the wet area is expected to expand significantly from 15.9% in the historical period to 26.7% and 32.5% by the end of the twenty-first-century projection under the RCP4.5 and RCP8.5 (not shown) emission scenarios, respectively. Different from the rapid warming over global land regions, the direction of projected changes in precipitation extremes is different in the tropics, subtropics, and extratropical regions (shown in Fig. 5). Generally speaking, slight positive trends occur in Asia, Europe, North America, and tropical Africa and negative trends (drying) occur in southern Africa, South America, and Australia. However, statistically significant trends in monthly precipitation at the two-sided p value of 0.05 level are restricted to relatively small areas within these land regions. Similar to the projected precipitation amount (Knutti and Sedláček 2013), projected extreme precipitation events in CMIP5 models have larger uncertainties compared to temperature. Compared to the projected trends in soil moisture (Sheffield 2008; based on CMIP3 models), the wetting trends in South America, eastern Africa, and western Australia are coincident with statistically significant increasing trends in soil moisture, suggesting the dominant role of precipitation in controlling soil moisture content

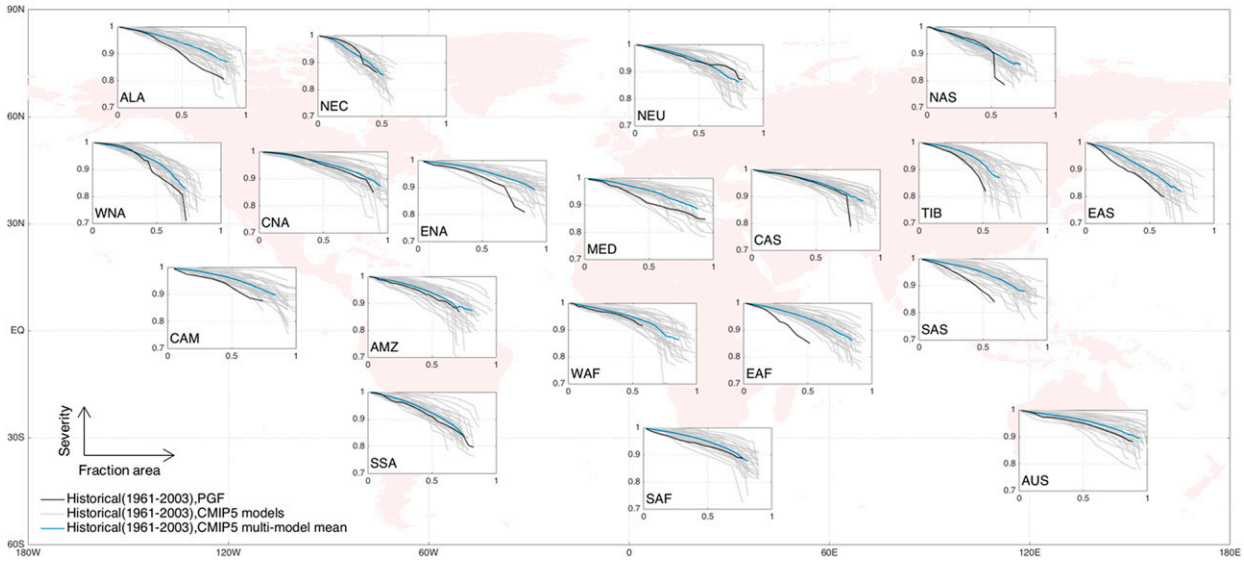

FIG. 3. The 3-month SAD curves for 1-sigma dry extremes in the historical period (1961–2003) from CMIP5 single model (gray line) and multimodel ensemble mean (blue line) as compared to PGF (black line).

in these regions despite the increasing evapotranspiration driven by higher temperatures (Vicente-Serrano et al. 2014; Berg and Sheffield 2018). Similar to the asymmetry found in the projected temperature distribution, projected changes in the seasonal variability of precipitation extremes also vary by season. During JJA, there is a smaller increase in both the lower and upper tails for monthly precipitation as compared to the DJF months. This suggests a smaller increase in JJA precipitation variability than DJF precipitation when compared to their variability in the historical period.

We next investigate trends in the characteristics (occurrence, magnitude, and severity) of the regional largest dry and wet events in the twenty-first century.

1) DRY EVENTS

The predicted future changes in short-term drought occurrence are generally decreasing in many regions, as is shown in the statistics in Table S2. In general, dry events are more persistent in the future projections when compared to the historical period. This is indicated by a decrease in the number of short-term (1–6-month

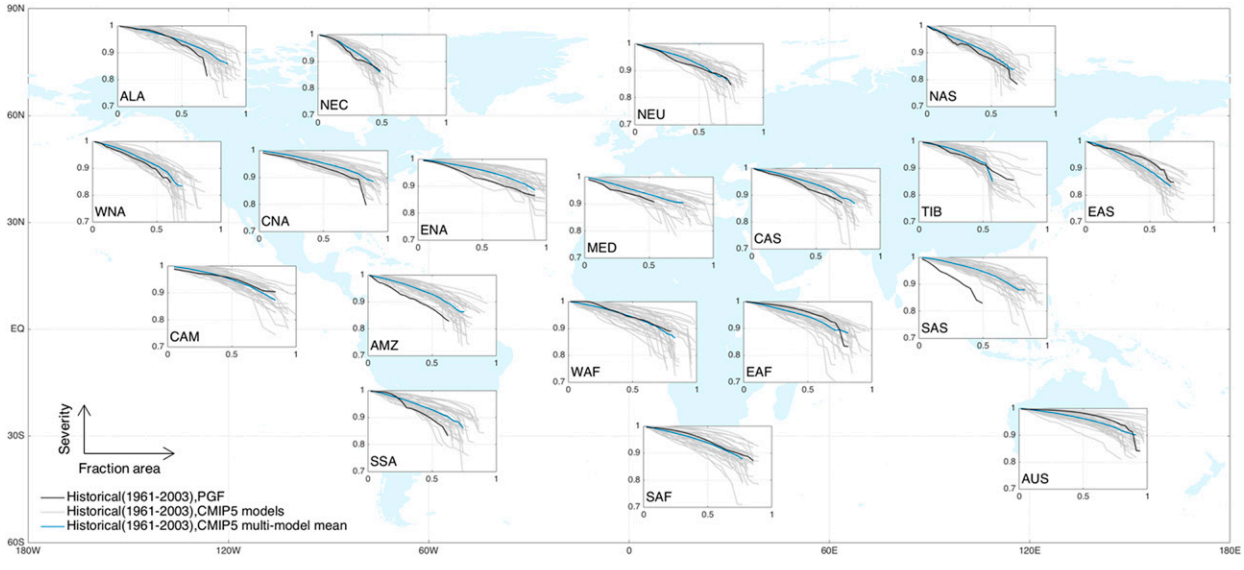

FIG. 4. As in Fig. 3, but for wet extremes.

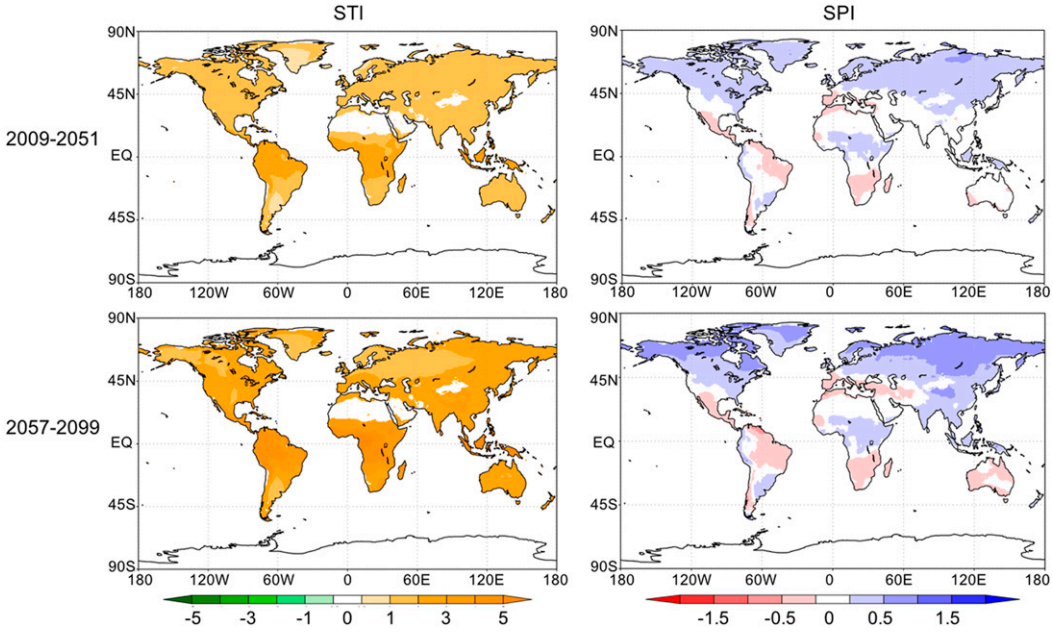

FIG. 5. Spatial patterns of global temperature and precipitation changes as indicated in mean STI and SPI in the near term (2009–51) and long term (2057–99) under the RCP4.5 emission scenario.

duration) droughts and an increase in the occurrence of mid (7–12-month duration) to long-term (12+-month duration) droughts. Increased drought frequency is seen in CAM and MED regions for both scenarios regardless of drought duration. These regions coincide with the regions projected to have lower average SPI in the future. In other words, drought clusters in regions that are projected to be drier (decreasing monthly precipitation) will experience more frequent dry extremes, especially short-term events with smaller spatial extents. However, in SAF, where SPI is also projected to decrease in the future, there will be more midterm to long-term events with larger spatial extents. A large part of Asia and Europe, including NAS, SAS, EAS, TIB, and NEU, will have fewer drought events. Note that precipitation in NAS will decrease in the mean while there is little change in mean precipitation in SAS. This suggests a decrease in the mean and an increase in variability in NAS, whereas in SAS there is only increasing variability but little change in the mean value. In addition, decreasing drought occurrence also applies for AUS and CNA.

Changes in the estimated maximum extent of the most temporally and spatially extensive dry/wet events from CMIP5 models are shown in Fig. 6. Regions that are expected to experience significant decreases in temporal persistence and spatial extent include ALA, EAS, NAS, ENA, NEC, TIB, and NEU. Slight increases in the magnitude of temporal and spatial extent are found in AMZ, SAF, AUS, and CAM. This is consistent with our analysis in the projected trends in precipitation.

Figure 7 shows the projected 3-month SAD curves of dry extremes at the global scale for short-term and long-term simulations. Results demonstrate that in the high-latitude regions, such as ALA, NEC, and NAS, maximum severity will decrease across spatial scales. Specifically, decreases can be found in NAS and NEC in the coming decades during the first half of the twenty-first century without further decreases in the second half of the twenty-first century. In ALA, the maximum severity of drought events will continue to decrease after the 2009–51 period. Overall, differences between the RCP4.5 and RCP8.5 emission scenarios are small. The midlatitude regions in the Northern Hemisphere (WNA, CAN, ENA, MED, CAS, TIB, EAS, SAS) show little change in maximum severity, which is not true in the RCP8.5 high-emission scenario from 2057 to 2099. This also applies to tropical Africa (WAF and EAF) and AUS. However, no statistically significant changes are found in these regions under the RCP4.5 scenario. Regions that will experience more severe droughts include CAM, AMZ, and SAF across all the spatial scales, which is due to an increase in the drought center severity with relatively similar severity gradient with respect to area. Major differences appear in the magnitude of severity increase across scenarios, as we increase the emission level from moderate to high. Such scenario dependence confirms recent findings

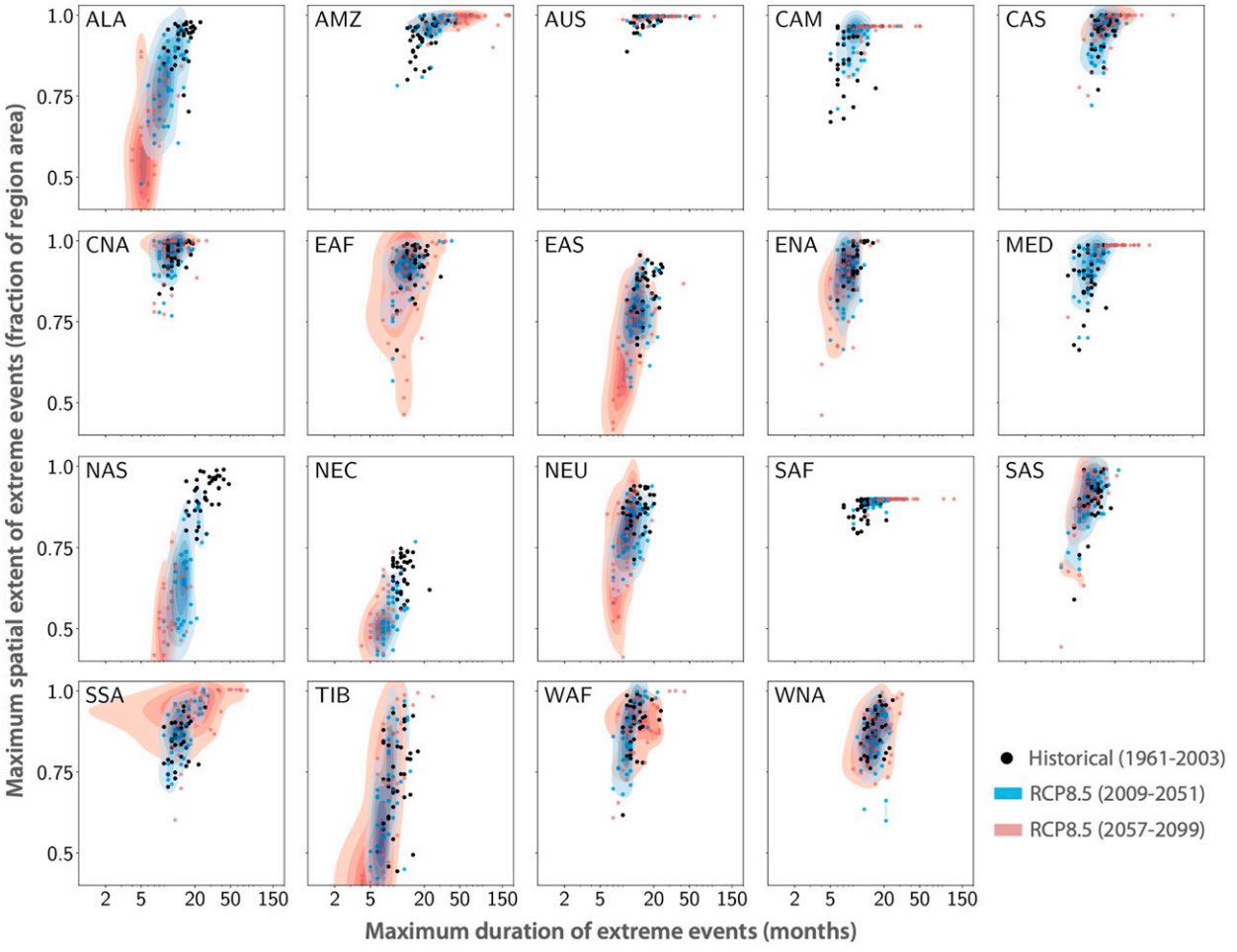

FIG. 6. Projected maximum temporal duration and maximum spatial extent of dry extreme events in the near term (2009–51) and long term (2057–99) in CMIP5 models compared to the historical period (1961–2003).

by Alden et al. (2016). In the meantime, it also provides further evidence that increases of seasonal dry extremes in the Amazon, as indicated by the 3-month SPI, are correlated with the rate of increasing temperature and the global carbon budget.

The SAD curves in Fig. 7 summarize the highest severity of the extreme events across different spatial scales. However, the event that contributes to the SAD curve at different spatial scales might be different since different events have different severity at the "event center" and with a different severity gradient as we expand around the center. We further examine the seasonal timing of the contributing events at different spatial scales (Fig. 8), comparing the historical timing with the observations and for the future period under RCP8.5. For the RCP8.5 scenario, major changes are found in the timing when the most severe events occur across spatial scales in a number of regions, while the RCP4.5 scenario (not shown) exhibits similar characteristics. Out of the three regions in the high latitudes, namely ALA, NEC, and NAS, with increasing drought severity, the timing of the most severe drought events will most likely shift in NAS from autumn/winter to spring/summer. In the historical period, the most severe drought events occur around October according to PGF, which are well reproduced by the CMIP5 models. For the long-term projection (2057–99), September droughts will increase in severity and start to exceed the severity of March droughts at small spatial extents near the drought center in the short-term (2009–51) projection. By the end of the twenty-first century under the RCP8.5 emission scenario, September droughts will have the highest severity across all spatial scales up to the maximum spatial extent of drought events.

No significant changes in the timing of the most severe events are observed in CAM, AMZ, and SAF as the maximum drought severity increases. The three

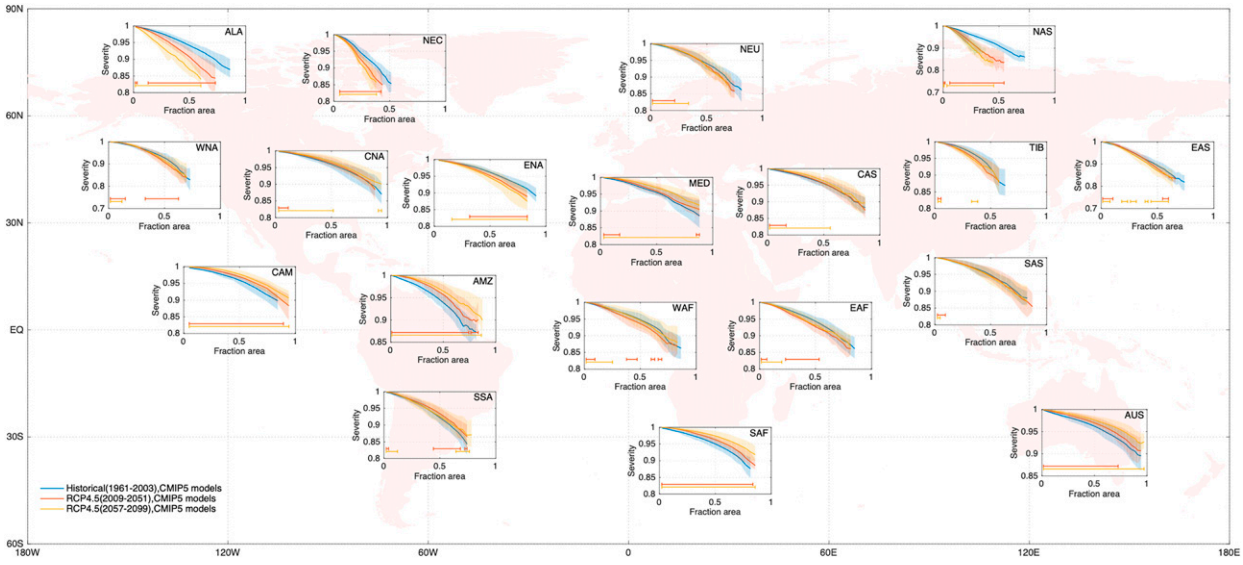

FIG. 7. Projected 3-month SAD curves of dry extremes in the near term (2009–51) and long term (2057–99) in CMIP5 models under RCP4.5 scenarios compared to the historical period (1961–2003). The shaded area represents one standard deviation from multimodel mean. Lines in the bottom of each panel indicate the spatial scales at which changes in severity are statistically significant at the 95% confidence interval in the two-sample Kolmogorov–Smirnov test between CMIP5 ensembles and PGF. Results showing the differences between RCP4.5 and RCP8.5 can be found in Fig. S5 in the online supplemental material.

regions would suffer from more severe droughts in the same drought-prone seasons than the historical period. However, this does not apply for a number of midlatitude and tropical regions, including WNA, SSA, MED, NEU, and SAS. Although there are no significant changes in the maximum drought severity, the timing of the most severe events most likely will shift; for example, from autumn (August–October) to spring (February–March) in WNA, and from autumn (around May) to early summer (October–December) in SSA. Notably, in SAS, more models agree that the most severe droughts are expected in the late season [September–November (SON)] as opposed to the early season [March–May (MAM)]. However, droughts in the early growing season will increase in severity according to the CMIP5 simulations. The early-season drought severity will exceed

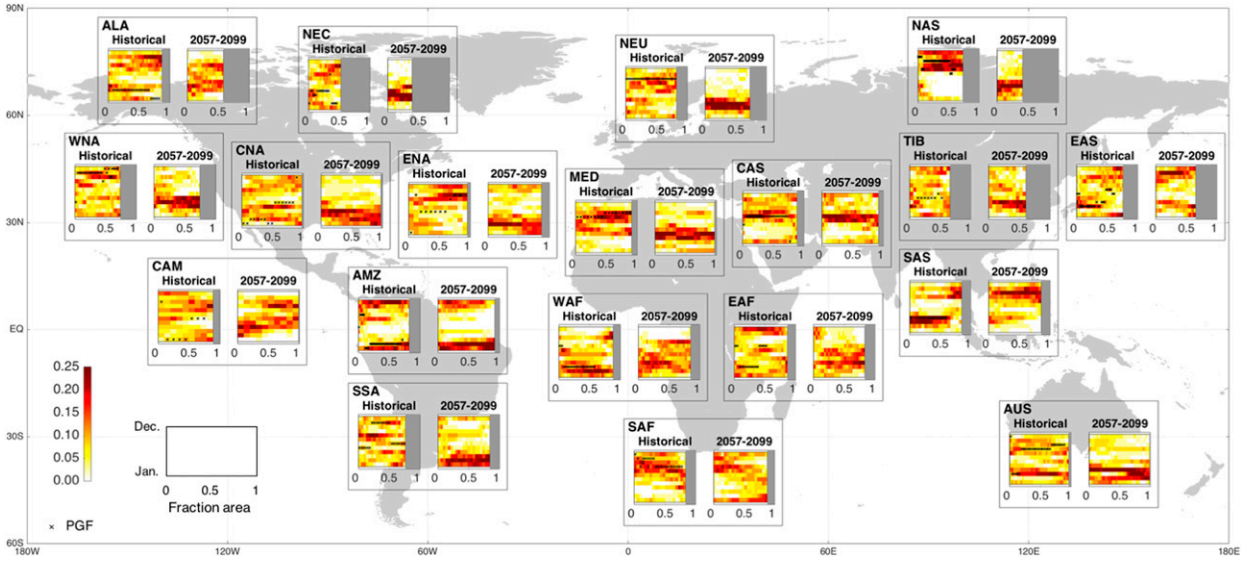

FIG. 8. Timing of the dry extreme events contributing to the 3-month SAD curves as in Fig. 6 for the historical period (1961–2003, left) and long-term (2057–99, right) future projections from CMIP5 models (RCP8.5 scenario). Color shading represents the percentage of models that predict (project) the same months of the most severe drought event.

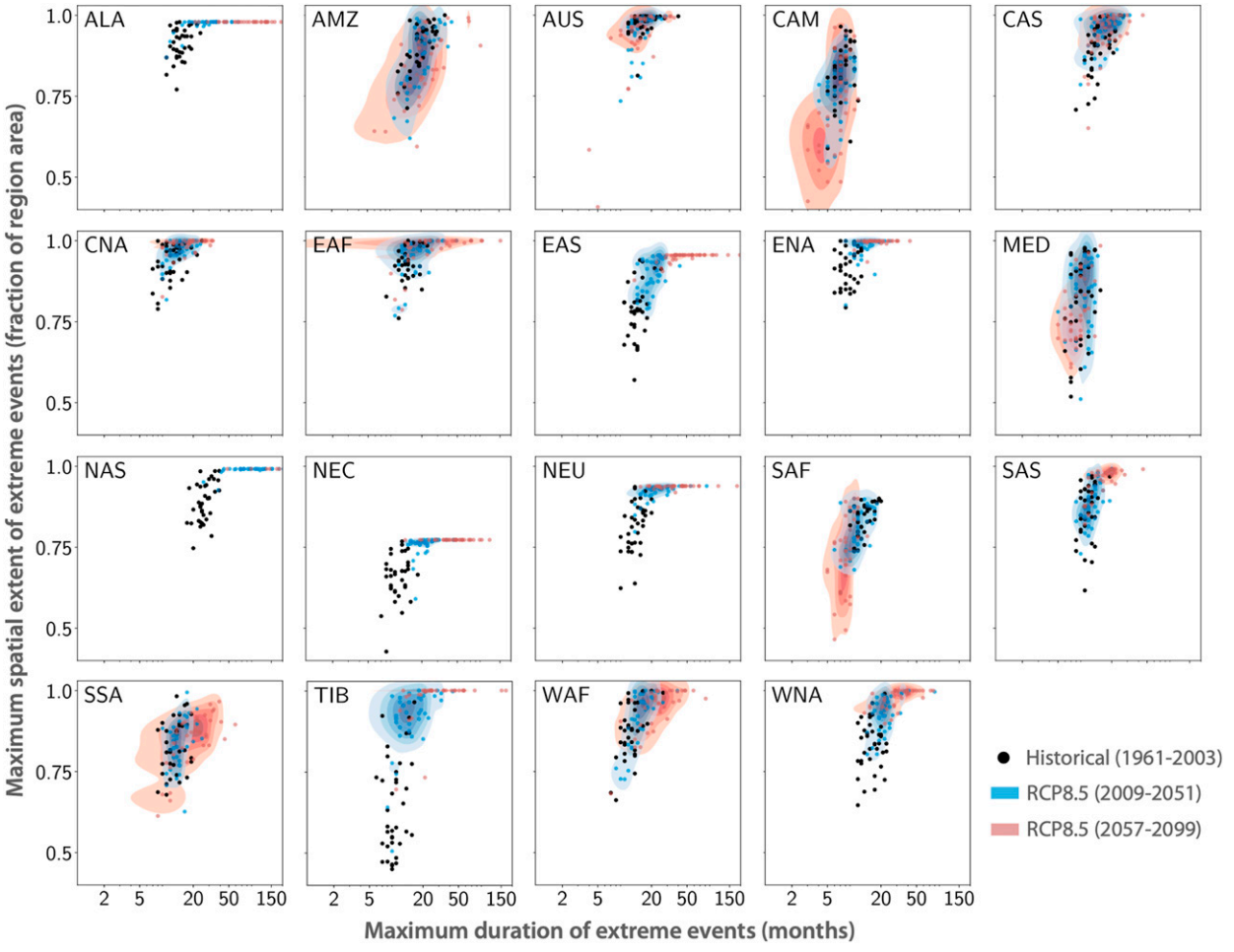

FIG. 9. As in Fig. 6, but for wet extremes.

the late-season severity at mid to large spatial scales by the end of the twenty-first century.

2) WET EVENTS

Similar to the changes in drought occurrence, as indicated from the statistics in Table S2, the wet events in the twenty-first century will also be more temporally persistent. Most regions will expect less short-term wet events, except CNA, ENA, TIB, SAS, and MED. In all regions except for NAS, the number of mid- to long-term wet events will increase. Changes in the frequency of wet events in the NAS region appear to be different from the rest of the global land area, with less wet events of short to middle duration in the twenty-first century. This is because NAS will aggressively extend both spatially and temporally due to its largest projected increases in precipitation, resulting in more long-term wet extremes especially during the first half of the twenty-first century. Figure 9 shows the projected change in maximum temporal and spatial extent for wet events. The maximum spatial extent of wet events almost covers the entire NAS region by the end of the twenty-first century under the RCP4.5 emission scenario. Furthermore, this projection is consistent across all 37 CMIP5 climate models included in this study. The regions with increasing drought extent (e.g., CAM, AMZ, SAF, and AUS) will have little or small decrease in maximum extent for wet events in the twenty-first century. Meanwhile, mid- to high-latitude regions with decreasing drought extent will expect larger and longer wet events in the future, along with tropical and Southern Hemisphere regions with no significant changes in drought extent. The magnitude of the increase in temporal and spatial wet extent is larger than the magnitude of the relative decrease of drought extent.

Comparison between Fig. 10 and Fig. 7 demonstrates that there is a larger increase in the severity of wet extremes covering more regions as opposed to dry events. In general, there is a north-to-south decreasing trend as the magnitude of severity increases. As mentioned before, NAS has the largest increase of drought severity.

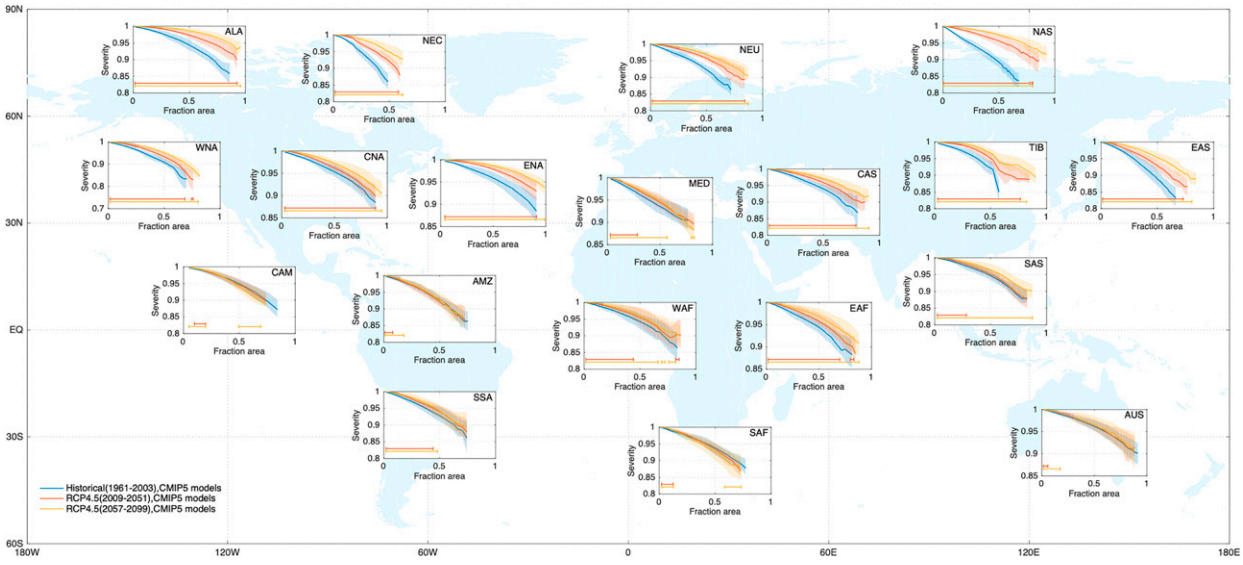

FIG. 10. As in Fig. 7, but for wet extremes. Results showing the differences between RCP4.5 and RCP8.5 can be found in Fig. S6 in the online supplemental material.

However, unlike dry events, the magnitude of severity for wet extremes exhibits relatively large interscenario difference, suggesting that the wet extremes in NAS are more consistent with greenhouse gas emissions than dry events. We can most likely expect a severity increase as soon as the coming decades in the first half of the twenty-first century (2009–51). Other regions in high latitudes, including ALA, NEC, and NEU, exhibit strong wet extremes, followed by parts of tropical Africa (i.e., EAF and midlatitude regions including EAS, TIB, CAS, ENA, CNA, and WNA). It is worth noting that regions with decreasing means in seasonal precipitation (indicated by SPI3; not shown here) are not projected to experience smaller wet severity. Instead, decreases in wet conditions appear to manifest through a large decrease in the maximum spatial extent, while the increase in wet conditions will lead to increasing event severity as well as maximum spatial and temporal extent.

The seasonal timing of the most severe wet events changes little in the Northern Hemisphere across different spatial scales (Fig. 11). The lack of skill in estimating the observed timing by the CMIP5 models in AMZ, MED, SAF, and AUS makes it difficult to conclude timing shifts with high confidence. However, the SAS region stands out with fairly high level of consensus from more than 25% of CMIP5 models in changes in timing. In the historical period the most severe wet events at mid to large spatial scale occur during the austral spring months (i.e., September–October). Summer [June–August (JJA)] wet extremes only take up a small part of the SAD curve at small spatial scales, which are projected to change in the future under both RCP4.5 and RCP8.5 emission scenarios. That is, during the late summer to autumn months, the severity of the most intense wet events exceeds that of the spring events, especially in the second half of the twenty-first century under the RCP8.5 emission scenario. Compared with the expected change of the dry events as discussed in section 4c(1), southern China will be subject to large impacts that will further impact agriculture yield production in the near future. This is further discussed in section 5.

d. Projected future changes in concurrent events

Further insights can be obtained through coincidence analysis of the concurrent dry/wet and hot/cold events. We use the SAD clustering algorithm to first identify precipitation extremes (dry/wet events). Based on their temporal span and spatial extent, we then calculate the aggregated temperature anomalies at the event level based on STI. This enables us to further classify the dry/wet extremes into three temperature categories: hot ($\mathrm{STI} \geq 1$), normal ($-1 < \mathrm{STI} < 1$), and cold ($\mathrm{STI} \leq -1$). The fractional change in the joint occurrence of concurrent dry/wet and hot/cold events during the near-term (2009–51) and long-term (2057–99) projection period is compared with the historical period (1961–2003) as a baseline. Results shown in Fig. 12 indicate substantial increases in the occurrence of joint dry/hot and wet/hot combinations for the projection period under both RCP4.5 and RCP8.5 emission scenarios. This indicates increased precipitation variability coupled with the warmed temperature, as has already been observed in the second half of the twentieth century (Hao et al. 2013). Little change is found in the

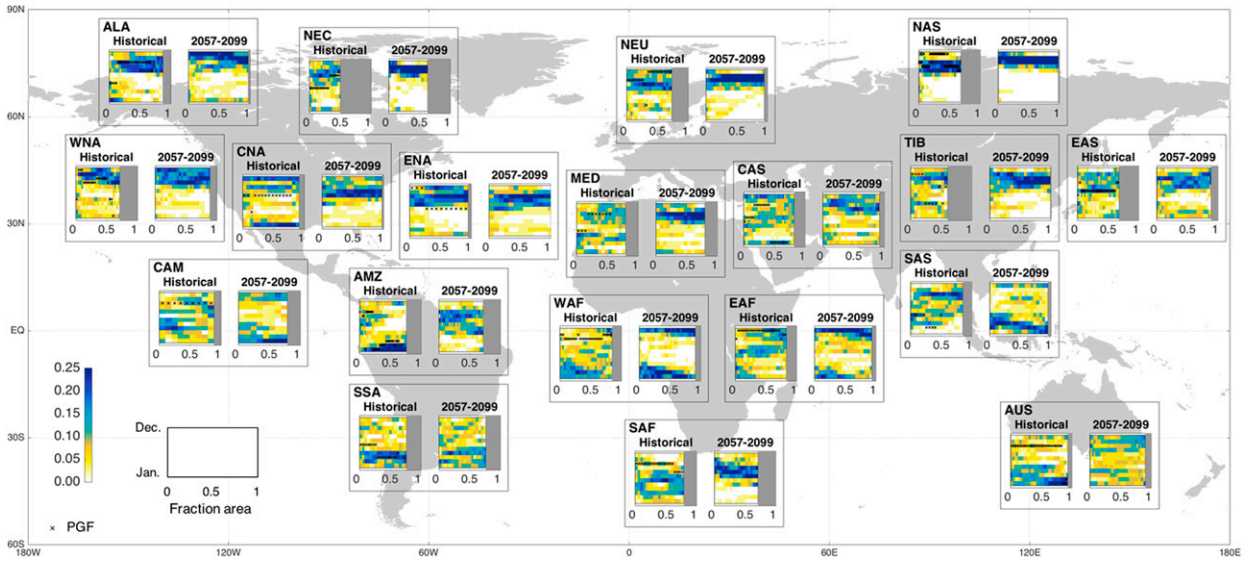

FIG. 11. As in Fig. 8, but for wet extremes.

occurrence of dry/cold events while a small decrease in wet/cold event occurrence is expected in the Southern Hemisphere, suggesting an asymmetric change in the precipitation distribution with a longer upper tail. In addition, changes in wet/hot extremes are more pronounced than dry/hot extremes, especially in the Northern Hemisphere. In the Amazon and Australia, little increase in wet extremes is projected while increase in wet/hot extremes are expected. This illustrates that changes in the rate of concurrent extremes can be driven by temperature trends. This could also be caused by the changes in the dependence structure between precipitation and temperature under climate change, which has been demonstrated by Zhou and Liu (2018) over China. The differences in the occurrence between wet/hot and dry/hot extremes could also be related to other factors, including large-scale climate signals [such as El Niño–Southern Oscillation (ENSO) and Pacific decadal oscillation; S. Wang et al. 2014; Sun et al. 2016], land–atmosphere coupling (e.g., Seneviratne and Stockli 2008; Lorenz et al. 2015), and urbanization (e.g., Sun et al. 2014), which requires further investigation into the complex relationship between these factors and the occurrence of these concurrent extremes.

5. Conclusions and discussion

In general, the statistics of the spatial–temporal characteristics of precipitation and temperature extremes presented in this study suggest confidence in the CMIP5 archived models to reproduce the statistics of observed dry/wet and hot/cold events in the historical period. Results show significant changes in the frequency of dry/wet and hot/cold events, as well as the severity and spatial and temporal extent of the precipitation and temperature extremes in the twenty-first century.

Trends in temperature in the twenty-first century are dominated by a rapid mean temperature increase of 2.84° and 4.45°C under RCP4.5 and RCP8.5 scenarios, respectively. On average, the global mean precipitation has a small wetting trend indicated by an average increase in SPI3 of 0.17 and 0.23 by the end of the twenty-first century under RCP4.5 and RCP8.5 scenarios, respectively. In addition, regional precipitation variability is projected to increase. Increases in rainfall variability are most significant in the tropics and Southern Hemisphere, where the enhanced precipitation distribution is indicated by intensification of dry and wet extremes. Specifically, dry and wet events are projected to be more temporally correlated, since the number of mid- to long-term events is projected to increase while the number of short-term events is projected to decrease. Furthermore, analysis of the severity, maximum temporal duration, and spatial extent shows that for dry extremes, high-latitude regions such as ALA, NEC, NEU, and NAS will decrease in maximum severity across different spatial scales as well as the maximum temporal and spatial extent. The Southern Hemisphere, in contrast, will have more severe dry extremes with marginally larger severity. The most significant changes for dry extremes are associated with the timing when the most severe events occur. For instance, large parts of Asia including NAS, EAS, and SAS are projected to experience a shift in the timing of dry extremes. For wet events, the maximum extent of the extreme events will increase in most of the land regions both temporally and spatially. The SAD curves

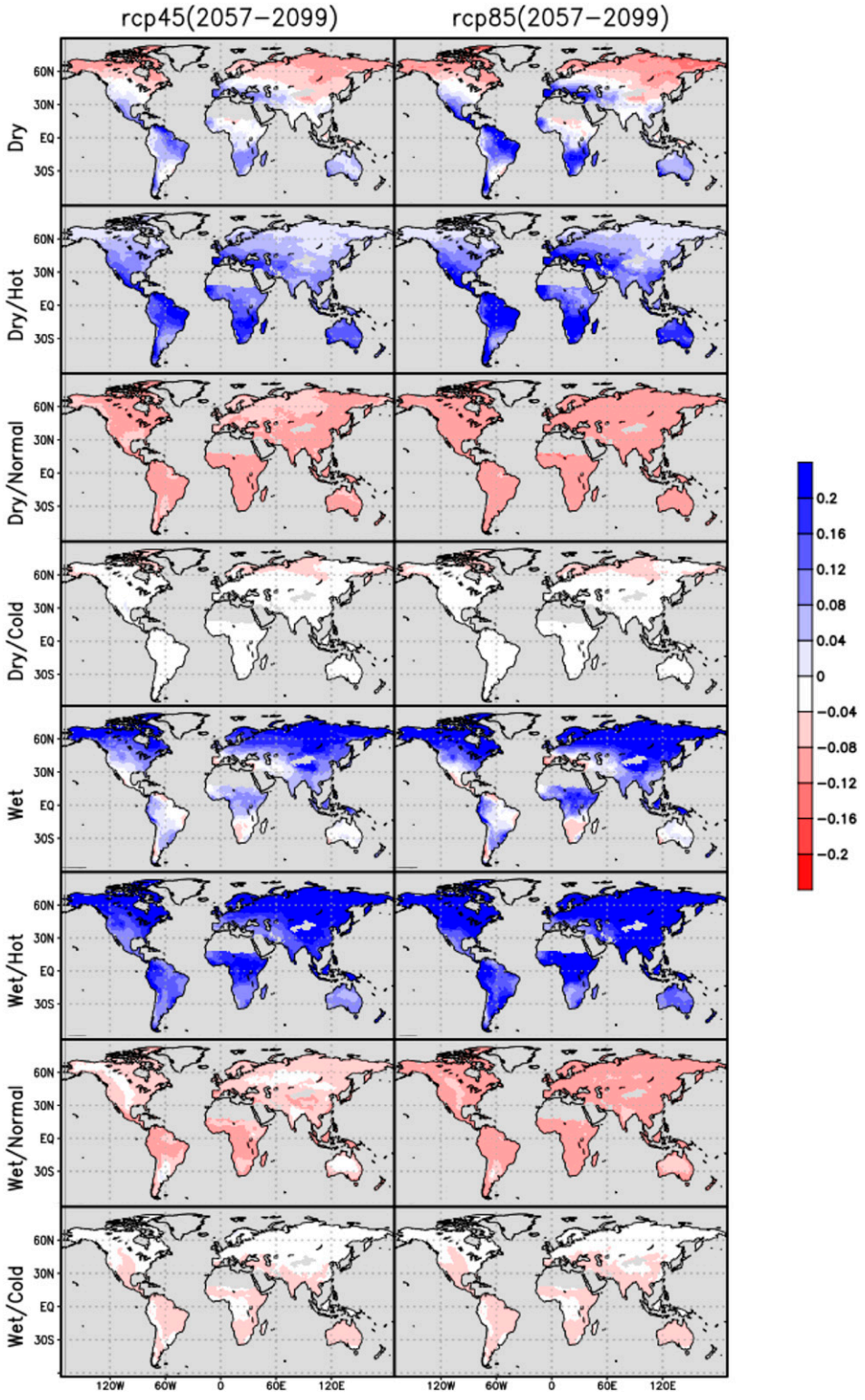

FIG. 12. Fractional changes in the occurrences of the dry/wet, hot/normal/cold, and concurrent extreme events for the near term (2009–51) and long term (2057–99) in CMIP5 model simulations under RCP4.5 and RCP8.5 scenarios.

indicate a significant increase in the high-latitude regions regardless of emission scenarios. On the other hand, these regions show little changes in the timing of the most severe events. However, the timing shift is most evident in the tropical regions (e.g., SAS).

a. *Changes in hydrological regime in response to climate change*

The International Panel on Climate Change's Special Report on Extremes (Karl et al. 2008; IPCC 2012) presented the scenarios of future shifts in temperature and precipitation extremes. The simplified scenarios include three aspects: shifted mean, increased variability, and changed symmetry. Here we summarize the results of this study under this framework in Fig. 13 based on the analyzed characteristics of the extreme events in the 37-member ensemble of CMIP5 GCMs identified by the SPI3 and SAD analysis. This is in contrast to the IPCC SREX regional analysis of climate extremes that is based on daily maximum temperature and daily precipitation rate. Consistent with IPCC (2012), the future temperature distribution is projected to have a large increase in the mean. In addition, the temperature distribution is projected to have a relatively smaller increase in variability. The increase in spread is consistent with an increase in the rate of the warming trend (Huntingford et al. 2013), which is asymmetric with a longer upper tail and relatively shorter lower tail. For the precipitation projections, the magnitude of the mean shift is smaller than the increase of variability. Differences between the RCP4.5 and RCP8.5 emission scenarios mainly lie in the fatter upper tail (i.e., larger, longer, and more severe wet extremes). In addition, precipitation projections change across different latitudes. The Northern Hemisphere and the tropics will experience a wetting trend with the former having more wet extremes. This is consistent with the projected changes in heavy daily precipitation events in the Northern Hemisphere found in IPCC (2012). The Southern Hemisphere, on the other hand, will have more dry extremes with a slight decrease in the mean precipitation.

b. *Concurrent temperature and precipitation extreme events*

It is well recognized that temperature and precipitation are dependent on each other (Adler et al. 2008). Changes in temperature and precipitation, together, affect soil moisture, which in turn impacts precipitation and temperature through land–atmosphere interactions. In the past 60 years, there has been little change in soil moisture drought events at the global scale (Sheffield et al. 2012). However, it is likely that soil moisture drought in the twenty-first century will intensify in parts of Europe,

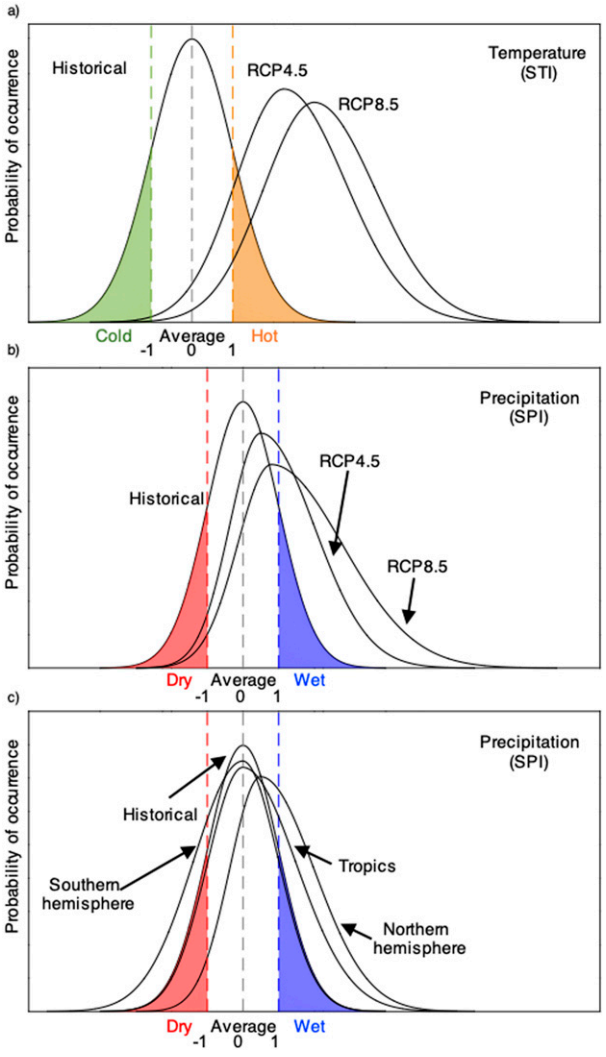

FIG. 13. Changes in the probability distribution of (a) temperature and (b) precipitation extremes under different emission scenarios (RCP4.5 and RCP8.5) in the Northern Hemisphere and (c) changes in precipitation extremes across different latitudinal regions under RCP4.5.

central North America, Central America and Mexico, northeast Brazil, and southern Africa (Seneviratne et al. 2012; Dai 2013; Orlowsky and Seneviratne 2013). This could be explained by soil moisture–atmosphere coupling (Jaeger and Seneviratne 2011) and the increasing probability of occurrence of joint dry/hot events (shown in Fig. 12).

c. *Intermodel variability*

In this study, we examine the fidelity of CMIP5 climate models to reproduce observed characteristics of precipitation and temperature extremes. Our results suggest moderate skill in estimating the characteristics of the dry/wet and hot/cold extremes. Larger

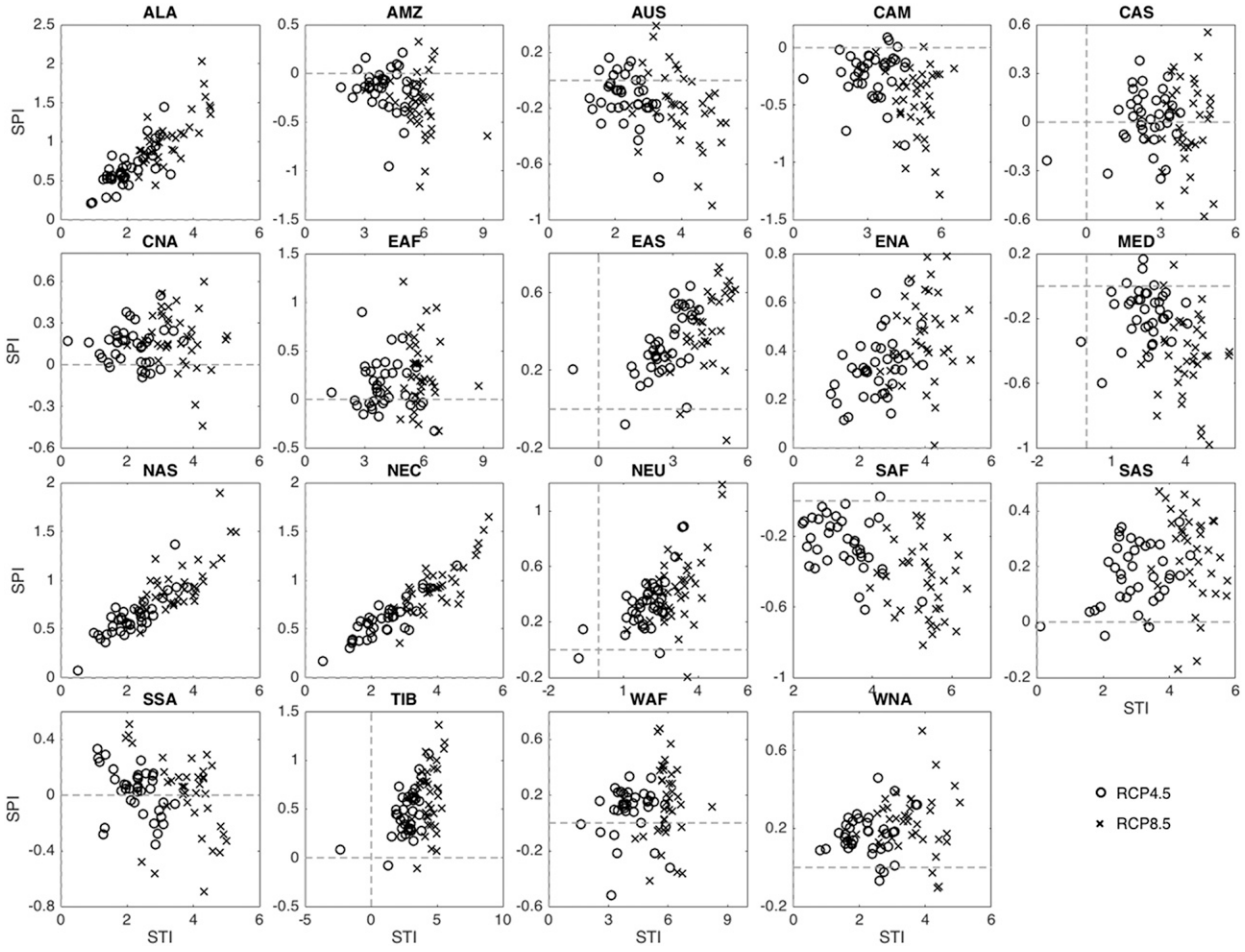

FIG. 14. Projected changes in mean STI and mean SPI between 2057–99 and 1961–2003 under RCP4.5 and RCP8.5 emission scenarios in global land regions.

discrepancies are found in the simulated timing of the most severe events, as discussed in section 4. However, as shown in Fig. 14 (corresponding statistics are provided in Tables S3 and S4), most models agree on the direction of change in temperature and precipitation in the twenty-first century. A few models project the opposite direction in precipitation change compared to the majority of models, including the GFDL climate models (GFDL-ESM2M, GFDL-ESM2G, GFDL CM3), CSIRO climate models (CSIRO-Mk3, CSIRO-Mk3.6.0), and FIO-ESM. Regions with the largest uncertainties in precipitation projections are located mainly in Oceania and South America. This highlights the need to improve the physical process representation in global climate models and select a subset of climate models to produce more robust future simulations based on their historical performance (Evans et al. 2013).

d. *Intercomparison of scenarios*

For both dry and wet extremes, minor differences appear in the direction of changes across models and across scenarios, while larger differences appear in the increasing magnitude under different emissions scenarios. The median of the CMIP5 model projections for the twenty-first century across the RCP4.5 and RCP8.5 scenarios examined agrees in more substantial changes in extreme events as a result of the higher emission. Precipitation changes under these two scenarios generally have the same sign, but higher changes are usually associated with higher greenhouse gas emissions. In particular, model projections for three specific regions (i.e., CAS, WAF, and SSA) fail to agree on the direction of precipitation changes under both RCP4.5 and RCP8.5 scenarios.

e. *Future work*

The SAD analysis results depend on the definition of the regions. In this study, we adopted the 19 subcontinental regions defined by Giorgi and Francisco (2000). However, some of the observed and modeled events have spatial extents that span the boundaries of

the regions. Further studies focusing on the migration patterns of extreme events are recommended at continental scale. In this study, we investigated the concurrent precipitation and temperature events based on SAD analysis of precipitation and temperature indexes. The same method can be extended to investigate the joint probability of precipitation and temperature events based on bivariate indexes. For example, a bivariate extension of the SPI defined by Mahony and Cannon (2018) can be applied to analyze concurrent temperature and precipitation extremes. Furthermore, since the total grid area is dependent on latitude (at higher latitudes the area of a grid cell would be smaller than around the equator), further studies are encouraged to configure the model resolution based on grid area, or conduct sensitivity tests to examine how results might differ across different regions if using a varying threshold to identify the spatial clusters of extremes.

Climate extremes have posed unprecedented challenges to socioeconomic and natural systems through, for example, agricultural production (Lobell et al. 2008; Johansson et al. 2015) and water availability (Evans and Schreider 2002; Zhang et al. 2014). On top of the mean state of the climate system (e.g., temperature), the increase in the occurrence of climate extremes will further pose more severe threat on the agricultural production. One of the characteristics that requires further investigation is the impact of extreme events that occur at different growing stages over different extents. Changes in timing will have tremendous impact on yield production since the yield loss due to early and late season droughts can be vastly different (Jongdee 2003; Ma et al. 2013). For instance, our results suggest that southern Asia will have less severe droughts in the beginning of the growing season and more severe wet extremes during the late growing season. This is particularly critical since large areas in the southern China region grow rice, which is vital to national food security. While we recognize that estimated impacts on projected yields are subject to large uncertainties (Folberth et al. 2016), the results presented here suggest potential impacts given the strong link between drought, heatwaves, and crop production. The existence of model and scenario uncertainties, due to the lack of knowledge on climate change impact, accuracy of datasets and inadequate representation of climate mechanisms, poses substantial threats in these regions in terms of their climate adaptation capacity and thus have to be taken into account by policy makers to tackle the challenge of infrastructure planning and design.

Acknowledgments. This research was supported through NOAA Grant number NA14OAR4310218 (Development of a global flood and drought catalogue for the 20th and early 21st centuries based on improved assessment of the global terrestrial water cycle and its extremes).

REFERENCES

Adler, R. F., and Coauthors, 2003: The version-2 Global Precipitation Climatology Project (GPCP) monthly precipitation analysis (1979–present). *J. Hydrometeor.*, **4**, 1147–1167, https://doi.org/10.1175/1525-7541(2003)004<1147:TVGPCP>2.0.CO;2.

——, G. Gu, J.-J. Wang, G. J. Huffman, S. Curtis, and D. Bolvin, 2008: Relationships between global precipitation and surface temperature on interannual and longer timescales (1979–2006). *J. Geophys. Res.*, **113**, D22104, https://doi.org/10.1029/2008JD010536.

Alden, C. B., and Coauthors, 2016: Regional atmospheric CO_2 inversion reveals seasonal and geographic differences in Amazon net biome exchange. *Global Change Biol.*, **22**, 3427–3443, https://doi.org/10.1111/gcb.13305.

Alexander, L. V., 2016: Global observed long-term changes in temperature and precipitation extremes: A review of progress and limitations in IPCC assessments and beyond. *Wea. Climate Extremes*, **11**, 4–16, https://doi.org/10.1016/j.wace.2015.10.007.

Aloysius, N. R., J. Sheffield, J. E. Saiers, H. Li, and E. F. Wood, 2016: Evaluation of historical and future simulations of precipitation and temperature in central Africa from CMIP5 climate models. *J. Geophys. Res. Atmos.*, **121**, 130–152, https://doi.org/10.1002/2015JD023656.

Andreadis, K. M., E. A. Clark, A. W. Wood, A. F. Hamlet, and D. P. Lettenmaier, 2005: Twentieth-century drought in the conterminous United States. *J. Hydrometeor.*, **6**, 985–1001, https://doi.org/10.1175/JHM450.1.

Arnell, N. W., and S. N. Gosling, 2016: The impacts of climate change on river flood risk at the global scale. *Climatic Change*, **134**, 387–401, https://doi.org/10.1007/s10584-014-1084-5.

Barriopedro, D., E. M. Fischer, J. Luterbacher, R. M. Trigo, and R. García-Herrera, 2011: The hot summer of 2010: Redrawing the temperature record map of Europe. *Science*, **332**, 220–224, https://doi.org/10.1126/science.1201224.

Berg, A., and J. Sheffield, 2018: Climate change and drought: The soil moisture perspective. *Curr. Climate Change Rep.*, **4**, 180–191, https://doi.org/10.1007/s40641-018-0095-0.

Cannon, A. J., 2015: Selecting GCM scenarios that span the range of changes in a multimodel ensemble: Application to CMIP5 climate extremes indices. *J. Climate*, **28**, 1260–1267, https://doi.org/10.1175/JCLI-D-14-00636.1.

Cheng, L., T. J. Phillips, and A. AghaKouchak, 2015: Non-stationary return levels of CMIP5 multi-model temperature extremes. *Climate Dyn.*, **44**, 2947–2963, https://doi.org/10.1007/s00382-015-2625-y.

Dai, A., 2013: Increasing drought under global warming in observations and models. *Nat. Climate Change*, **3**, 52–58, https://doi.org/10.1038/nclimate1633.

de Vries, H., R. J. Haarsma, and W. Hazeleger, 2012: Western European cold spells in current and future climate. *Geophys. Res. Lett.*, **39**, L04706, https://doi.org/10.1029/2011GL050665.

Easterling, D. R., G. A. Meehl, C. Parmesan, S. Changnon, T. R. Karl, and L. O. Mearns, 2000: Climate extremes: Observations, modeling, and impacts. *Science*, **289**, 2068–2074, https://doi.org/10.1126/science.289.5487.2068.

Evans, J., and S. Schreider, 2002: Hydrological impacts of climate change on inflows to Perth, Australia. *Climatic Change*, **55**, 361–393, https://doi.org/10.1023/A:1020588416541.

——, F. Ji, G. Abramowitz, and M. Ekström, 2013: Optimally choosing small ensemble members to produce robust climate simulations. *Environ. Res. Lett.*, **8**, 044050, https://doi.org/10.1088/1748-9326/8/4/044050.

——, ——, C. Lee, P. Smith, D. Argüeso, and L. Fita, 2014: Design of a regional climate modelling projection ensemble experiment—NARCliM. *Geosci. Model Dev.*, **7**, 621–629, https://doi.org/10.5194/gmd-7-621-2014.

Folberth, C., R. Skalský, E. Moltchanova, J. Balkovič, L. B. Azevedo, M. Obersteiner, and M. van der Velde, 2016: Uncertainty in soil data can outweigh climate impact signals in global crop yield simulations. *Nat. Commun.*, **7**, 11872, https://doi.org/10.1038/ncomms11872.

Giorgi, F., and R. Francisco, 2000: Uncertainties in regional climate change prediction: A regional analysis of ensemble simulations with the HadCM2 coupled AOGCM. *Climate Dyn.*, **16**, 169–182, https://doi.org/10.1007/PL00013733.

Goswami, B. N., V. Venugopal, D. Sengupta, M. S. Madhusoodanan, and P. K. Xavier, 2006: Increasing trend of extreme rain events over India in a warming environment. *Science*, **314**, 1442–1445, https://doi.org/10.1126/science.1132027.

Hansen, J., M. Sato, and R. Ruedy, 2012: Perception of climate change. *Proc. Natl. Acad. Sci. USA*, **109**, E2415–E2423, https://doi.org/10.1073/pnas.1205276109.

Hao, Z., A. AghaKouchak, and T. J. Phillips, 2013: Changes in concurrent monthly precipitation and temperature extremes. *Environ. Res. Lett.*, **8**, 034014, https://doi.org/10.1088/1748-9326/8/3/034014.

——, V. Singh, and F. Hao, 2018: Compound extremes in hydroclimatology: A review. *Water*, **10**, 718, https://doi.org/10.3390/W10060718.

Harris, I., P. D. Jones, T. J. Osborn, and D. H. Lister, 2014: Updated high-resolution grids of monthly climatic observations—The CRU TS3.10 dataset. *Int. J. Climatol.*, **34**, 623–642, https://doi.org/10.1002/joc.3711.

He, X., L. Estes, M. Konar, D. Tian, D. Anghileri, K. Baylis, T. P. Evans, and J. Sheffield, 2019: Integrated approaches to understanding and reducing drought impact on food security across scales. *Curr. Opin. Environ. Sustain.*, **40**, 43–54, https://doi.org/10.1016/j.cosust.2019.09.006.

——, M. Pan, Z. Wei, E. F. Wood, and J. Sheffield, 2020: A global drought and flood catalogue from 1950 to 2016. *Bull. Amer. Meteor. Soc.*, https://doi.org/10.1175/BAMS-D-18-0269.1, in press.

Hirabayashi, Y., R. Mahendran, S. Koirala, L. Konoshima, D. Yamazaki, S. Watanabe, H. Kim, and S. Kanae, 2013: Global flood risk under climate change. *Nat. Climate Change*, **3**, 816–821, https://doi.org/10.1038/nclimate1911.

Huffman, G. J., and Coauthors, 2007: The TRMM Multisatellite Precipitation Analysis (TMPA): Quasi-global, multiyear, combined-sensor precipitation estimates at fine scales. *J. Hydrometeor.*, **8**, 38–55, https://doi.org/10.1175/JHM560.1.

Huntingford, C., P. D. Jones, V. N. Livina, T. M. Lenton, and P. M. Cox, 2013: No increase in global temperature variability despite changing regional patterns. *Nature*, **500**, 327–330, https://doi.org/10.1038/nature12310.

IPCC, 2012: *Managing the Risks of Extreme Events and Disasters to Advance Climate Change Adaptation*. Cambridge University Press, 582 pp.

——, 2013: Summary for policymakers. *Climate Change 2013: The Physical Science Basis*, T. F. Stocker et al., Eds., Cambridge University Press, 1–29.

Jaeger, E. B., and S. I. Seneviratne, 2011: Impact of soil moisture–atmosphere coupling on European climate extremes and trends in a regional climate model. *Climate Dyn.*, **36**, 1919–1939, https://doi.org/10.1007/S00382-010-0780-8.

Johansson, R., E. Luebehusen, B. Morris, H. Shannon, and S. Meyer, 2015: Monitoring the impacts of weather and climate extremes on global agricultural production. *Wea. Climate Extremes*, **10**, 65–71, https://doi.org/10.1016/j.wace.2015.11.003.

Jongdee, B., 2003: Designing a national breeding program for developing drought-tolerant rainfed lowland varieties: The Thailand experience. *Breeding Rice for Drought-Prone Environments*, K. S. Fischer et al., Eds., International Rice Research Institute, 64–69.

Karl, T. R., G. A. Meehl, C. D. Miller, S. J. Hassol, A. M. Waple, and W. L. Murray, 2008: *Weather and Climate Extremes in a Changing Climate: Regions of Focus: North America, Hawaii, Caribbean, and U.S. Pacific Islands.* U.S. Climate Change Science Program, 162 pp.

Kharin, V. V., F. W. Zwiers, X. Zhang, and M. Wehner, 2013: Changes in temperature and precipitation extremes in the CMIP5 ensemble. *Climatic Change*, **119**, 345–357, https://doi.org/10.1007/s10584-013-0705-8.

Knutti, R., and J. Sedláček, 2013: Robustness and uncertainties in the new CMIP5 climate model projections. *Nat. Climate Change*, **3**, 369–373, https://doi.org/10.1038/nclimate1716.

Kodra, E., and A. R. Ganguly, 2014: Asymmetry of projected increases in extreme temperature distributions. *Sci. Rep.*, **4**, 5884, https://doi.org/10.1038/SREP05884.

——, K. Steinhaeuser, and A. R. Ganguly, 2011: Persisting cold extremes under 21st-century warming scenarios. *Geophys. Res. Lett.*, **38**, L08705, https://doi.org/10.1029/2011GL047103.

Leonard, M., and Coauthors, 2014: A compound event framework for understanding extreme impacts. *Wiley Interdiscip. Rev.: Climate Change*, **5**, 113–128, https://doi.org/10.1002/WCC.252.

Lobell, D. B., and S. M. Gourdji, 2012: The influence of climate change on global crop productivity. *Plant Physiol.*, **160**, 1686–1697, https://doi.org/10.1104/pp.112.208298.

——, M. B. Burke, C. Tebaldi, M. D. Mastrandrea, W. P. Falcon, and R. L. Naylor, 2008: Prioritizing climate change adaptation needs for food security in 2030. *Science*, **319**, 607–610, https://doi.org/10.1126/science.1152339.

Lorenz, R., and Coauthors, 2015: Influence of land–atmosphere feedbacks on temperature and precipitation extremes in the GLACE-CMIP5 ensemble. *J. Geophys. Res. Atmos.*, **121**, 607–623, https://doi.org/10.1002/2015JD024053.

Ma, X., S. Wu, Y. E. Li, X. Zhang, Q. Gao, and Y. Wu, 2013: Rice re-cultivation in southern China: An option for enhanced climate change resilience in rice production. *J. Geogr. Sci.*, **23**, 67–84, https://doi.org/10.1007/s11442-013-0994-x.

Mahony, C. R., and A. J. Cannon, 2018: Wetter summers can intensify departures from natural variability in a warming climate. *Nat. Commun.*, **9**, 783, https://doi.org/10.1038/s41467-018-03132-z.

McKee, T. B., N. J. Doesken, and J. Kleist, 1993: The relationship of drought frequency and duration to time scales. *Proc. Eighth Conf. on Applied Climatology*, Anaheim, CA, Amer. Meteor. Soc., 179–184.

Meehl, G. A., C. Covey, T. Delworth, M. Latif, B. McAvaney, J. F. B. Mitchell, R. J. Stouffer, and K. E. Taylor, 2007: The WCRP CMIP3 multimodel dataset: A new era in climate change research. *Bull. Amer. Meteor. Soc.*, **88**, 1383–1394, https://doi.org/10.1175/BAMS-88-9-1383.

Mendelsohn, R., A. Dinar, and L. Williams, 2006: The distributional impact of climate change on rich and poor countries.

Environ. Dev. Econ., **11**, 159–178, https://doi.org/10.1017/S1355770X05002755.

Mideksa, T. K., and S. Kallbekken, 2010: The impact of climate change on the electricity market: A review. *Energy Policy*, **38**, 3579–3585, https://doi.org/10.1016/j.enpol.2010.02.035.

Milly, P. C. D., R. T. Wetherald, K. Dunne, and T. L. Delworth, 2002: Increasing risk of great floods in a changing climate. *Nature*, **415**, 514–517, https://doi.org/10.1038/415514a.

Moftakhari, H. R., G. Salvadori, A. AghaKouchak, B. F. Sanders, and R. A. Matthew, 2017: Compounding effects of sea level rise and fluvial flooding. *Proc. Natl. Acad. Sci. USA*, **114**, 9785–9790, https://doi.org/10.1073/pnas.1620325114.

Nakicenovic, N., and R. Swart, Eds., 2000: *Special Report on Emissions Scenarios*. Cambridge University Press, 612 pp.

New, M., M. Hulme, and P. Jones, 2000: Representing twentieth-century space-time climate variability. Part II: Development of 1901–96 monthly grids of terrestrial surface climate. *J. Climate*, **13**, 2217–2238, https://doi.org/10.1175/1520-0442(2000)013<2217:RTCSTC>2.0.CO;2.

Orlowsky, B., and S. I. Seneviratne, 2013: Elusive drought: Uncertainty in observed trends and short-and long-term CMIP5 projections. *Hydrol. Earth Syst. Sci.*, **17**, 1765–1781, https://doi.org/10.5194/hess-17-1765-2013.

Palmer, T. N., 2013: Climate extremes and the role of dynamics. *Proc. Natl. Acad. Sci. USA*, **110**, 5281–5282, https://doi.org/10.1073/pnas.1303295110.

Sarhadi, A., M. C. Ausín, M. P. Wiper, D. Touma, and N. S. Diffenbaugh, 2018: Multidimensional risk in a nonstationary climate: Joint probability of increasingly severe warm and dry conditions. *Sci. Adv.*, **4**, eaau3487, https://doi.org/10.1126/sciadv.aau3487.

Seneviratne, S. I., and R. Stockli, 2008: The role of land–atmosphere interactions for climate variability in Europe. *Climate Variability and Extremes During the Past 100 Years*, S. Brönnimann et al., Eds., Springer, 179–193.

——, and Coauthors, 2012: Changes in climate extremes and their impacts on the natural physical environment. *Managing the Risks of Extreme Events and Disasters to Advance Climate Change Adaptation*, C. B. Field et al., Eds., Cambridge University Press, 109–230.

Sheffield, J., 2008: Global drought in the 20th and 21st centuries: Analysis of retrospective simulations and future projections of soil moisture. Ph.D. thesis, Wageningen University, 206 pp.

——, and E. F. Wood, 2008: Projected changes in drought occurrence under future global warming from multi-model, multi-scenario, IPCC AR4 simulations. *Climate Dyn.*, **31**, 79–105, https://doi.org/10.1007/s00382-007-0340-z.

——, G. Goteti, and E. F. Wood, 2006: Development of a 50-year high-resolution global dataset of meteorological forcings for land surface modeling. *J. Climate*, **19**, 3088–3111, https://doi.org/10.1175/JCLI3790.1.

——, E. F. Wood, and M. L. Roderick, 2012: Little change in global drought over the past 60 years. *Nature*, **491**, 435–438, https://doi.org/10.1038/nature11575.

——, and Coauthors, 2013a: North American climate in CMIP5 experiments. Part I: Evaluation of historical simulations of continental and regional climatology. *J. Climate*, **26**, 9209–9245, https://doi.org/10.1175/JCLI-D-12-00592.1.

——, and Coauthors, 2013b: North American climate in CMIP5 experiments. Part II: Evaluation of historical simulations of intraseasonal to decadal variability. *J. Climate*, **26**, 9247–9290, https://doi.org/10.1175/JCLI-D-12-00593.1.

Sillmann, J., V. V. Kharin, X. Zhang, F. W. Zwiers, and D. Bronaugh, 2013a: Climate extremes indices in the CMIP5 multimodel ensemble: Part 1. Model evaluation in the present climate. *J. Geophys. Res. Atmos.*, **118**, 1716–1733, https://doi.org/10.1002/jgrd.50203.

——, ——, F. W. Zwiers, X. Zhang, and D. Bronaugh, 2013b: Climate extremes indices in the CMIP5 multimodel ensemble: Part 2. Future climate projections. *J. Geophys. Res. Atmos.*, **118**, 2473–2493, https://doi.org/10.1002/jgrd.50188.

Stackhouse, P. W., S. K. Gupta, S. J. Cox, J. C. Mikovitz, T. Zhang, and M. Chiacchio, 2004: 12-year surface radiation budget data set. *GEWEX News*, No. 14 (4), International GEWEX Project Office, Silver Spring, MD, 10–12.

Stern, N., 2013: The structure of economic modeling of the potential impacts of climate change: Grafting gross underestimation of risk onto already narrow science models. *J. Econ. Lit.*, **51**, 838–859, https://doi.org/10.1257/jel.51.3.838.

Sun, Q., C. Miao, A. AghaKouchak, and Q. Duan, 2016: Century-scale causal relationships between global dry/wet conditions and the state of the Pacific and Atlantic Oceans. *Geophys. Res. Lett.*, **43**, 6528–6537, https://doi.org/10.1002/2016GL069628.

Sun, Y., X. Zhang, F. W. Zwiers, L. Song, H. Wan, T. Hu, H. Yin, and G. Ren, 2014: Rapid increase in the risk of extreme summer heat in eastern China. *Nat. Climate Change*, **4**, 1082–1085, https://doi.org/10.1038/nclimate2410.

Taylor, K. E., R. J. Stouffer, and G. A. Meehl, 2012: An overview of CMIP5 and the experiment design. *Bull. Amer. Meteor. Soc.*, **93**, 485–498, https://doi.org/10.1175/BAMS-D-11-00094.1.

Tebaldi, C., and R. Knutti, 2007: The use of the multi-model ensemble in probabilistic climate projections. *Philos. Trans. Roy. Soc. London*, **365A**, 2053–2075, https://doi.org/10.1098/rsta.2007.2076.

Thomson, A. M., and Coauthors, 2011: RCP4.5: A pathway for stabilization of radiative forcing by 2100. *Climatic Change*, **109**, 77–94, https://doi.org/10.1007/s10584-011-0151-4.

Toreti, A., and Coauthors, 2013: Projections of global changes in precipitation extremes from Coupled Model Intercomparison Project Phase 5 models. *Geophys. Res. Lett.*, **40**, 4887–4892, https://doi.org/10.1002/grl.50940.

Trenberth, K. E., 2011: Changes in precipitation with climate change. *Climate Res.*, **47**, 123–138, https://doi.org/10.3354/CR00953.

——, J. T. Fasullo, and T. G. Shepherd, 2015: Attribution of climate extreme events. *Nat. Climate Change*, **5**, 725–730, https://doi.org/10.1038/nclimate2657.

van Vuuren, D. P., and Coauthors, 2011: The representative concentration pathways: An overview. *Climatic Change*, **109**, 5–31, https://doi.org/10.1007/s10584-011-0148-z.

Vicente-Serrano, S. M., and Coauthors, 2014: Evidence of increasing drought severity caused by temperature rise in southern Europe. *Environ. Res. Lett.*, **9**, 044001, https://doi.org/10.1088/1748-9326/9/4/044001.

Vidal, J.-P., E. Martin, N. Kitova, J. Najac, and J.-M. Soubeyroux, 2012: Evolution of spatio-temporal drought characteristics: Validation, projections and effect of adaptation scenarios. *Hydrol. Earth Syst. Sci.*, **16**, 2935–2955, https://doi.org/10.5194/hess-16-2935-2012.

Wang, A., D. P. Lettenmaier, and J. Sheffield, 2011: Soil moisture drought in China, 1950–2006. *J. Climate*, **24**, 3257–3271, https://doi.org/10.1175/2011JCLI3733.1.

Wang, C., L. Zhang, S.-K. Lee, L. Wu, and C. R. Mechoso, 2014: A global perspective on CMIP5 climate model biases. *Nat. Climate Change*, **4**, 201–205, https://doi.org/10.1038/nclimate2118.

Wang, S., J. Huang, Y. He, and Y. Guan, 2014: Combined effects of the Pacific decadal oscillation and El Niño–Southern Oscillation on global land dry–wet changes. *Sci. Rep.*, **4**, 6651, https://doi.org/10.1038/srep06651.

Westra, S., L. V. Alexander, and F. W. Zwiers, 2013: Global increasing trends in annual maximum daily precipitation. *J. Climate*, **26**, 3904–3918, https://doi.org/10.1175/JCLI-D-12-00502.1.

Wheeler, T., and J. Von Braun, 2013: Climate change impacts on global food security. *Science*, **341**, 508–513, https://doi.org/10.1126/science.1239402.

WMO, 2012: Standardized precipitation index user guide. WMO-1090, 24 pp., http://www.wmo.int/pages/prog/wcp/agm/publications/agm_proceedings.php.

Zhan, W., K. Guan, J. Sheffield, and E. F. Wood, 2016: Depiction of drought over sub-Saharan Africa using reanalysis precipitation datasets. *J. Geophys. Res. Atmos.*, **121**, 10 555–10 574, https://doi.org/10.1002/2016JD024858.

Zhang, X., L. Alexander, G. C. Hegerl, P. Jones, A. Klein Tank, T. C. Peterson, B. Trewin, and F. W. Zwiers, 2011: Indices for monitoring changes in extremes based on daily temperature and precipitation data. *Wiley Interdiscip. Rev.: Climate Change*, **2**, 851–870, https://doi.org/10.1002/wcc.147.

——, G. Hegerl, S. Seneviratne, R. Stewart, F. Zwiers, and L. Alexander, 2014: WCRP grand challenge: Understanding and predicting weather and climate extremes. Tech. Rep., 10 pp., https://www.wcrp-climate.org/images/documents/grand_challenges/GC_Extremes_v2.pdf.

Zhou, P., and Z. Liu, 2018: Likelihood of concurrent climate extremes and variations over China. *Environ. Res. Lett.*, **13**, 094023, https://doi.org/10.1088/1748-9326/aade9e.

Zscheischler, J., and S. I. Seneviratne, 2017: Dependence of drivers affects risks associated with compound events. *Sci. Adv.*, **3**, e1700263, https://doi.org/10.1126/sciadv.1700263.

——, and Coauthors, 2014: Impact of large-scale climate extremes on biospheric carbon fluxes: An intercomparison based on MsTMIP data. *Global Biogeochem. Cycles*, **28**, 585–600, https://doi.org/10.1002/2014GB004826.